AGU PUBLICATIONS

JGR

Journal of Geophysical Research: Solid Earth

RESEARCH ARTICLE
10.1002/2016JB013850

Pitfalls in modeling mantle convection with internal heat production

Jun Korenaga[1]

[1]Department of Geology and Geophysics, Yale University, New Haven, Connecticut, USA

Key Points:
- Convection modeling with the mixed heating mode requires great care
- Careless model design prevents the application of simulation results to Earth's evolution
- A list of common pitfalls are provided, with a suggested strategy for how to avoid them

Correspondence to:
J. Korenaga,
jun.korenaga@yale.edu

Citation:
Korenaga, J. (2017), Pitfalls in modeling mantle convection with internal heat production, *J. Geophys. Res. Solid Earth*, *122*, 4064–4085, doi:10.1002/2016JB013850.

Received 29 JUL 2016
Accepted 6 MAY 2017
Accepted article online 11 MAY 2017
Published online 27 MAY 2017

Abstract The mantle of the Earth, and probably of other terrestrial planets as well, is heated from below and within. The heating mode of mantle convection is thus mixed heating, and it is also time dependent because the amount of heat-producing isotopes in the mantle is steadily decreasing by radioactive decay and because the basal heat flux originating in the cooling of the core can vary with time. This mode of transient mixed heating presents its own challenges to the study of mantle convection, but such difficulties are not always appreciated in the recent literature. The purpose of this tutorial is to clarify the issue of heating mode by explaining relevant concepts in a coherent manner, including the internal heating ratio, the Urey ratio, secular cooling, and the connection between the thermal budget of the Earth and the geochemical models of the Earth. The importance of such basic concepts will be explained with some illustrative examples in the context of the thermal evolution of the Earth, and a summary of common pitfalls will be provided, with a possible strategy for how to avoid them.

1. Introduction

Convection in the Earth's mantle is different from the classical Rayleigh-Bénard convection in several important aspects, including rheology, heating mode, geometry, compressibility, phase transition, and chemical differentiation [e.g., *Bercovici et al.*, 2000; *Schubert et al.*, 2001]. The primary focus of this paper is on the heating mode of mantle convection, although other aspects such as rheology and geometry are also discussed when they are essential to certain problems on heating mode. Whereas the fluid is only heated from below in the Rayleigh-Bénard convection, internal heating is also present for the case of the mantle owing to the decay of radioactive isotopes. Mantle convection is not purely basally heated nor purely internally heated; it is somewhere between these end-members, and its heating mode is often called mixed heating. Moreover, mantle convection is essentially transient, i.e., the internal temperature of the mantle is steadily changing with time (usually cooling down), and the secular cooling of the mantle can be regarded as additional internal heating [e.g., *Daly*, 1980; *Weinstein and Olson*, 1990]. The heating mode of mantle convection is thus mixed as well as transient.

Recent years have witnessed a growing number of mantle convection studies aiming at understanding the long-term evolution of the Earth and other terrestrial planets [e.g., *O'Neill and Lenardic*, 2007; *Shahnas et al.*, 2008; *Landuyt and Bercovici*, 2009; *O'Farrell and Lowman*, 2010; *Deschamps et al.*, 2010; *Korenaga*, 2010a; *Nakagawa and Tackley*, 2012; *Stein et al.*, 2013; *Noack and Breuer*, 2014; *Foley and Bercovici*, 2014; *Weller et al.*, 2015; *Lourenço et al.*, 2016; *Wong and Solomatov*, 2016], and a proper understanding of the evolving heating mode has become more important than ever. Unfortunately, however, the relevance of the heating mode tends to be overlooked in recent studies, making it difficult to assess their implications for planetary evolution. This is not surprising because it is not always straightforward to design convection models with a realistic mixed heating mode and correctly interpret modeling results; it requires a good understanding of both geodynamics and geochemistry. Although heating mode is just one aspect of mantle convection, it is connected directly to the dynamics of the top and bottom thermal boundary layers, which is central to the question of how a terrestrial planet evolves through mantle convection. Moreover, multidisciplinary research has become common in Earth and planetary sciences, and studies on the evolution of the early Earth and exoplanets are not an exception to the trend. For such problems with limited observational constraints, geodynamical studies can play a critical role by providing a physics-based foundation, which may help other disciplines. Yet, such a foundation could easily be shaken by mistreatment of heating mode. The purpose of this paper is therefore to clarify this issue of heating mode by organizing relevant concepts and common pitfalls in a coherent

manner and by providing some illustrative examples. To this end, I provide a review on heating mode based on the available literature as well as with the aid of simple convection simulations. As no previous study has performed such an exercise to my knowledge, my objective is to offer an insight into the heating mode of the mantle for future geodynamical studies.

The structure of the paper is as follows. I will first explain the basics of thermal convection with an emphasis on heating mode. Steady state solutions will be used to illustrate some subtle points associated with mixed heating and transient solutions to highlight the importance of secular cooling. As the amount of radiogenic heating is determined by the concentration of radioactive isotopes within the Earth, it is necessary to understand relevant geochemical concepts, which will be explained next. Whereas all numerical examples given in this paper are with Cartesian boxes, using the spherical shell geometry becomes essential to address certain types of convection problems, and this issue is also discussed. To demonstrate the importance of understanding the heating mode, I will then discuss two popular notions regarding how higher heat production in the past might have affected the evolution of the Earth. I will close with a summary of pitfalls and a possible strategy for how to avoid them.

2. Basics

2.1. Some Definitions

The nondimensionalized governing equations for thermal convection of an incompressible fluid consist of the conservation of mass,

$$\nabla \cdot \mathbf{u}^* = 0, \tag{1}$$

the conservation of momentum,

$$-\nabla P^* + \nabla \cdot \left[\eta^* \left(\nabla \mathbf{u}^* + \nabla \mathbf{u}^{*T}\right)\right] + RaT^* \mathbf{e}_z = 0, \tag{2}$$

and the conservation of energy,

$$\frac{\partial T^*}{\partial t^*} + \mathbf{u}^* \cdot \nabla T^* = \nabla^2 T^* + H^*. \tag{3}$$

The Cartesian geometry is assumed in sections 2.1 through 2.3; the effect of spherical geometry is discussed in section 2.5. The unit vector pointing upward is denoted by $\mathbf{e}_z$. Asterisks denote nondimensional variables. The spatial coordinates are normalized by the system depth D, and time is normalized by the diffusion timescale, D^2/κ, where κ is thermal diffusivity. Velocity $\mathbf{u}^*$ is thus normalized by κ/D. Dynamic pressure P^* and viscosity η^* are normalized by $\eta_0\kappa/D^2$ and η_0, respectively, where η_0 is a reference viscosity at T^*=1 (see equation (9)). Temperature T^* is normalized by a characteristic temperature scale ΔT. The Rayleigh number Ra is defined as

$$Ra = \frac{\alpha \rho_0 g \Delta T D^3}{\kappa \eta_0}, \tag{4}$$

where α is thermal expansivity, ρ_0 is reference density, and g is gravitational acceleration. The Rayleigh number is a nondimensional parameter. Heat generation H^* is defined as

$$H^* = \frac{\rho_0 H D^2}{k \Delta T}, \tag{5}$$

where H is heat production rate per unit mass, and k is thermal conductivity.

For purely internal heating, the temperature scale exhibited by a convection system is not known a priori. A common choice is to use the temperature scale derived from thermal conduction with heat generation,

$$\Delta T_H = \frac{\rho_0 H D^2}{k}. \tag{6}$$

For a purely conducting layer of thickness of D with uniform heat generation H and no basal heat flux, the total temperature variation across the layer is given by half of this temperature scale [e.g., *Turcotte and Schubert*, 2014, section 4.6]. Moreover, the use of the reference viscosity η_0, when defined at T^* = 1, is not guaranteed

to be a representative viscosity, and the Rayleigh number for purely internal heating is often defined with the surface viscosity, η_s, and the above temperature scale. Such a Rayleigh number is called the surface Rayleigh number, which may be expressed as

$$Ra_s = Ra\frac{\Delta T_H}{\Delta T}\frac{\eta_0}{\eta_s} = \frac{\alpha\rho_0^2 g H D^5}{k\kappa\eta_s}. \tag{7}$$

At the same time, the temperature scale ΔT_H is usually much greater than the actual temperature scale exhibited by a convecting system, and the convective potential measured by equation (7) differs from the scale given by equation (4). We thus often use another kind of Rayleigh number, the internal Rayleigh number, which is defined as

$$Ra_i = RaT_i^*\frac{\eta_0}{\eta_i} = \frac{\alpha\rho_0 g T_i^* \Delta T D^3}{\kappa\eta_i}, \tag{8}$$

where T_i^* denotes the internal temperature (normalized by ΔT), and η_i is the viscosity at the internal temperature. The exact definition of the internal temperature varies slightly among different studies [e.g., *Solomatov and Moresi*, 2000; *Korenaga*, 2009a], but it is meant to represent the average temperature of advection-dominated regions. The internal Rayleigh number is defined with the actual temperature scale as well as internal viscosity. The internal Rayleigh number can also be calculated for basal and mixed heating, in which case internal viscosity and temperature are measured away from both top and bottom boundary layers. The Rayleigh number given by equation (4) is also called the bottom (or basal) Rayleigh number as it is based on the viscosity at the bottom boundary where $T^* = 1$.

For simulation with purely internal heating, the temperature scale ΔT_H is sometimes used for nondimensionalization, in which case H^* becomes unity [e.g., *Solomatov and Moresi*, 2000]. To consider all types of heating modes collectively, however, it is more convenient to use the same temperature scale ΔT regardless of heating mode. I will thus use the bottom Rayleigh number Ra even for cases with purely internal heating, and it is to be understood that the temperature and viscosity scales assumed in the Rayleigh number are usually not realized in those cases. For example, if a purely internally heated case results in the internal temperature T_i^* of 0.8, the temperature contrast across the entire system is given simply by $T_i^*\Delta T = 0.8\Delta T$, where ΔT is the temperature scale assumed in the bottom Rayleigh number.

I will use three different kinds of viscosity in this paper: constant viscosity, temperature-dependent viscosity, and pseudoplastic rheology. The isoviscous cases (i.e., with constant viscosity) serve as the simplest examples, and the cases with temperature-dependent viscosity provide examples for stagnant lid convection. The cases with pseudoplastic rheology are used to simulate plate tectonic convection, i.e., the subduction of a strong top boundary layer. For temperature-dependent viscosity, the following linear exponential form is employed:

$$\eta_T^* = \exp[\theta(1 - T^*)], \tag{9}$$

where the Frank-Kamenetskii parameter, θ, controls the degree of temperature dependence. When T^* varies from 0 to 1, the total viscosity contrast achieved in the system is given by $\exp(\theta)$. This is a simplified form of the more realistic Arrhenius-type temperature dependence, and the parameter can be related to the activation energy E as

$$\theta = \frac{E\Delta T}{R(T_s + \Delta T)^2}, \tag{10}$$

where R is the universal gas constant and T_s is the surface temperature [e.g., *Solomatov and Moresi*, 2000]. For the present-day Earth's mantle, E is ~300 kJ mol^{-1} [e.g., *Karato and Wu*, 1993] and ΔT is ~1300 K (excluding the temperature contrast across the thermal boundary layer at the core-mantle boundary) [e.g., *Herzberg et al.*, 2007], so θ is ~20, which corresponds to a viscosity contrast of $\sim 5 \times 10^8$.

For cases with pseudoplastic rheology, I use the following nonlinear effective viscosity,

$$\eta_y^* = \frac{\tau_y^*}{e_{\mathrm{II}}^*}, \tag{11}$$

where τ_y^* is the constant (depth-independent) yield stress, and e_{II}^* is the second invariant of the strain rate tensor. The transition between plastic and ductile deformation is handled by using the harmonic mean of the temperature-dependent viscosity and the above effective viscosity as

$$\eta^* = \left(\frac{1}{\eta_T^*} + \frac{1}{\eta_y^*} \right)^{-1}. \tag{12}$$

For convection with basal and mixed heating, T^* is usually set to 0 at $z^* = 1$ (top) and 1 at $z^* = 0$ (bottom). For purely basal heating, H^* is 0, and total heat flow from the top is the same as total heat flow from the bottom, when averaged over a sufficient duration. The time-averaged heat flux from the top, q_t^*, is in general related to that from the bottom, q_b^*, as

$$q_t^* = q_b^* + H^*. \tag{13}$$

For convection with purely internal heating, the bottom boundary is insulated, i.e., $q_b^* = 0$.

It is convenient to introduce the internal heating ratio, ξ, defined as

$$\xi = \frac{H^*}{q_t^*} = \frac{q_t^* - q_b^*}{q_t^*}. \tag{14}$$

The ratio is 0 for purely basal heating, is unity for purely internal heating, and takes some other value for mixed heating. Using time-averaged heat fluxes from a statistically steady state solution is essential for equation (13) to hold. We can also calculate the ratio using instantaneous heat fluxes from a transient solution, using the right-hand definition of equation (14), but the instantaneous ratio does not necessarily have a clear connection to internal heating rate (section 2.3).

The Nusselt number is surface heat flux normalized by a hypothetical heat flux for a purely conductive system with the same temperature contrast across the convecting system, and for basal and mixed heating, we have

$$Nu = q_t^*, \tag{15}$$

because the total temperature contrast across the system is ΔT. For purely internal heating, we have instead

$$Nu = \frac{q_t^*}{T_i^*}, \tag{16}$$

because the temperature contrast is given by $T_i^* \Delta T$.

For purely internal heating, we can also define the Nusselt number using the temperature scale of ΔT_H, and in this case, the Nusselt number is given by $1/T_i^*$ (where T_i^* is normalized by ΔT_H) because the normalized heat production (and thus the nondimensional surface heat flux at a thermal equilibrium) becomes unity with ΔT_H. Note that for the case of purely internal heating, the Nusselt number can be expressed either as q_t^*/T_i^* with the temperature scale of ΔT or as $1/T_i^*$ with ΔT_H, but the value of the Nusselt number itself is unaffected by the choice of the temperature scale. Understanding these different definitions becomes important when using scaling relations developed in previous studies (section 2.3).

2.2. Steady State Solutions

There exist a number of classical studies in which we can see the consequences of different heating modes [e.g., *McKenzie et al.*, 1974; *Daly*, 1980; *Fleitout and Yuen*, 1984; *Christensen*, 1989], and a few representative snapshots from statistically steady state solutions are shown in Figure 1. These solutions are prepared as follows. The governing equations for thermal convection (equations (1)–(3)) are solved by the 2-D finite element code of *Korenaga and Jordan* [2003]. The top and bottom boundaries are free slip. The top temperature is fixed to 0. The bottom temperature is fixed to 1 for basal and mixed heating, whereas the bottom boundary is insulating for purely internal heating. A reflecting boundary condition (i.e., free slip and insulating) is applied to the side boundaries. The aspect ratio of a model is 4 to reduce wall effects, and the model is discretized by 256×64 uniform quadrilateral elements. Internal temperature is set to 1 at $t^* = 0$ with random perturbations of small amplitude (10^{-5}), and the system is integrated for a sufficiently long time (usually $t^* > 0.1$) to reach a statistically steady state. Two different viscosities are used: uniform viscosity (Figures 1a–1e) and

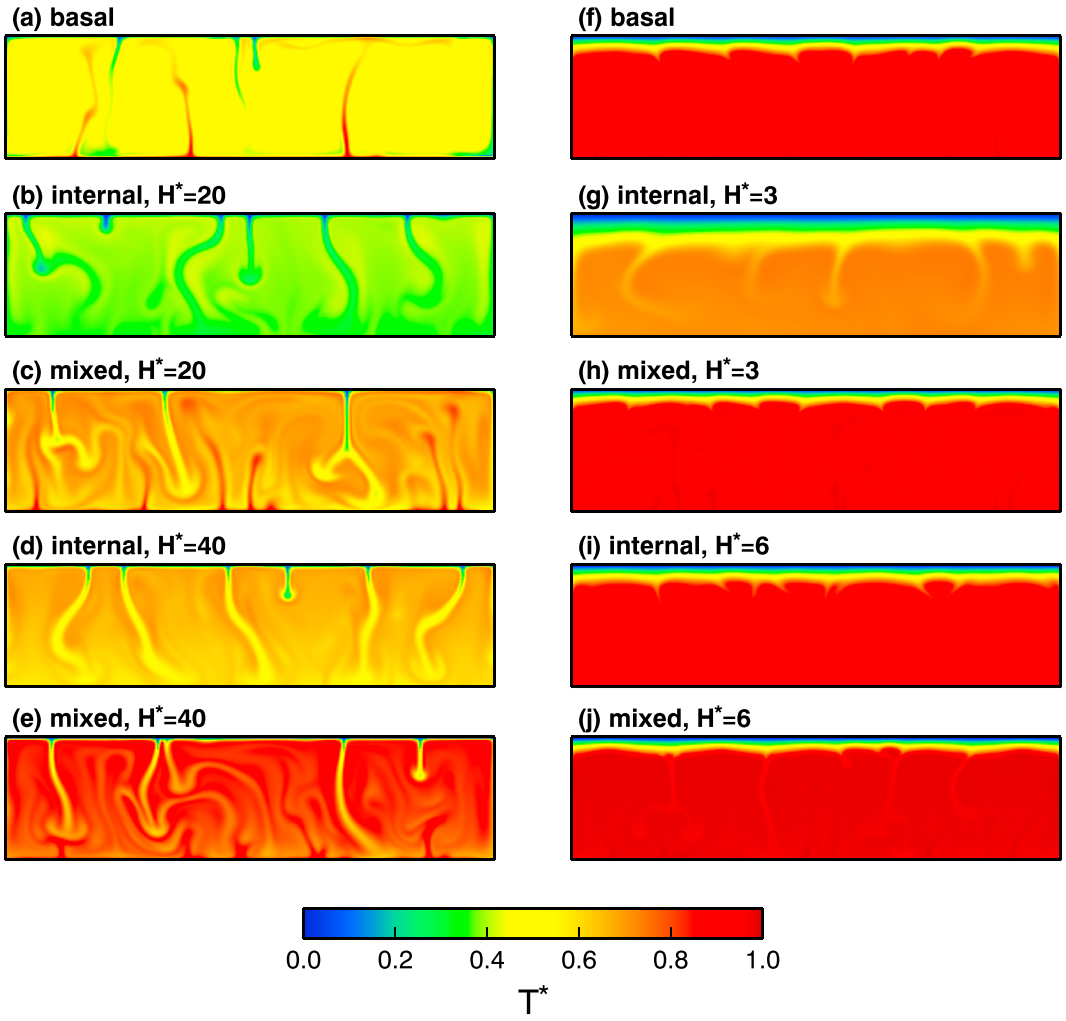

Figure 1. Temperature snapshots of steady state solutions with various heating modes. Columns include cases with (a–e) uniform viscosity (with $Ra = 10^7$) and (f–j) temperature-dependent viscosity (with $Ra = 3 \times 10^8$ and $\theta = 15$, so $\Delta\eta = \exp(15) \sim 3.3 \times 10^6$). For purely basal heating (Figures 1a and 1f), internal heating is 0, and for other cases, uniform internal heating is applied with the $H^* = 20$ (Figures 1b and 1c), 40 (Figures 1d and 1e), 3 (Figures 1g and 1h), and 6 (Figures 1i and 1j).

temperature-dependent viscosity with θ of 15 (Figures 1f–1j). The (bottom) Rayleigh number Ra is set to 10^7 for the former and 3×10^8 for the latter. The profiles of horizontally averaged temperature corresponding to these snapshots are shown in Figure 2.

The convection system exhibits a symmetric thermal structure only when viscosity is spatially uniform and heating is purely basal (Figures 1a and 2a). The internal temperature T_i^* is ~0.5, and the top and bottom boundary layers are similarly unstable. At the other extreme of purely internal heating, the bottom boundary layer is entirely absent (Figures 1b and 1d), and with a greater amount of internal heat production, the internal temperature increases (Figure 2a). The cases with mixed heating show higher internal temperature when compared with the same value of H^*, which is because of additional heat flux from the bottom. With greater H^*, downwellings from the top boundary layer become more dominant (Figures 1c and 1e). The internal heating ratios are ~0.46 and ~0.73 for the cases shown in Figures 1c and 1e, respectively. This effect of H^* should be understood with the fact that the isoviscous examples compared here are all obtained at the same Rayleigh number. Increasing the Rayleigh number, for example, would generally cool the fluid more efficiently, thereby reducing the effect of H^* on internal temperature [e.g., *Sotin and Labrosse*, 1999]. Scaling relations among heat flux, heat production, and internal temperature had been unavailable until recently for isoviscous convection with mixed heating [*Moore*, 2008; *Shahnas et al.*, 2008; *Choblet and Parmentier*, 2009; *O'Farrell and Lowman*, 2010; *Deschamps et al.*, 2010; *Choblet*, 2012].

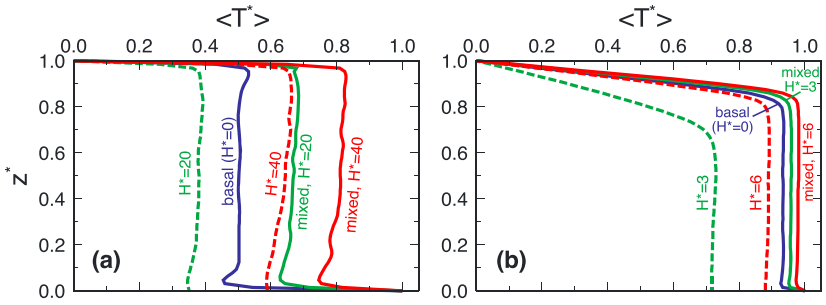

Figure 2. Horizontally averaged temperature corresponding to snapshots shown in Figure 1. (a) Cases with uniform viscosity. (b) Cases with temperature-dependent viscosity.

With strongly temperature-dependent viscosity, the top boundary layer carries a much greater temperature contrast than that in isoviscous cases (compare the left and right panels of Figure 1). All cases shown in Figures 1f–1j are in the regime of stagnant lid convection [e.g., *Solomatov*, 1995], in which the top boundary layer is too stiff to deform and convection can take place only beneath the rigid lid. The top boundary layer can become thick because of its stiffness, and cooling from above becomes inefficient. Compared to the isoviscous cases, therefore, the internal temperature is generally higher (Figure 2b), and so is the internal heating ratio; the values of ξ are ~0.47 and ~0.76, respectively, for H^* of only 3 and 6. For purely basal heating and purely internal heating, various scaling relations are available [e.g., *Moresi and Solomatov*, 1995; *Solomatov and Moresi*, 2000; *Reese et al.*, 2005; *Deschamps and Lin*, 2014; *Yao et al.*, 2014], and it is straightforward to design a simulation with a desired combination of surface heat flux and internal temperature. For mixed heating, such relations are yet to be developed, and it requires some trial and error to control surface heat flux, internal temperature, and internal heating ratio. In other words, with mixed heating, the overall temperature scale of the system is well defined because the bottom temperature is prescribed, but some important aspects such as the average temperature of the mantle, which is approximately T_i^*, and the relative importance of basal heat flux, which is related to ξ, can be determined only a posteriori and could vary in an unexpected manner depending on the assumed functionality of viscosity.

An example of such difficulty inherent to mixed heating is given in Figure 3. Here statistically steady state solutions are obtained using the pseudoplastic rheology of equation (12), with $\theta = 15$ and three different yield stresses τ_0^*: 1×10^9, 2×10^5, and 2×10^4. The bottom Rayleigh number is set to 10^7, and internal heating H^* is set to 3 in all of the three cases. When the yield stress is as high as 1×10^9, it does not compensate for the effect of temperature-dependent viscosity, and the system is in the regime of stagnant lid convection, with a high internal heating ratio (~0.83). When the yield stress is lowered to 2×10^5, the system exhibits episodic overturns of the top boundary layer [e.g., *Moresi and Solomatov*, 1998]. Most of the time, the system is in the stagnant lid regime, resembling very closely the situation depicted in Figure 3a, but occasionally, the top boundary layer becomes unstable (Figure 3b), and the subduction of the entire boundary layer temporally reduces the internal heating ratio to ~0.4, which then gradually recovers to the original high value (~0.83). Further reduction in the yield stress brings the system to the so-called mobile lid regime, in which the top boundary layer is constantly mobilized (Figure 3c). Because of efficient cooling in the mobile lid regime, the internal temperature is greatly reduced (~0.57), and the internal heating ratio is very low (~0.23). All of these cases share the identical bottom Rayleigh number ($Ra = 10^7$), the same amount of internal heating ($H^* = 3$), and the same viscosity contrast across the system due to temperature dependence ($\Delta\eta = \exp(15) \sim 3.3 \times 10^6$). Changing only one parameter, the yield stress, however, can bring drastic differences to the nature of convection; the mobile lid regime is characterized by a much colder mantle with more intensive basal heat flux than the other regimes. Also, the temperature drop across the top boundary layer in the mobile lid regime is nearly half of that in the episodic overturn and stagnant lid regimes. This indicates that the top boundary layer in the former is characterized by a considerably smaller viscosity contrast (~ 10^4; Figure 3, right panels). The nature of the top boundary layer (i.e., oceanic lithosphere) and the convecting interior is so different between the solutions shown in Figures 3b and 3c that if they represent different stages of planetary evolution as sometime assumed [e.g., *O'Neill et al.*, 2007], these stages must be vastly separated in time. For example, the internal temperature of Figure 3c is lower than that of Figure 3b by ~0.4, which is equivalent to ~800 K with ΔT of 2000 K (a typical temperature scale for the mantle convection of the Earth). For comparison, petrological

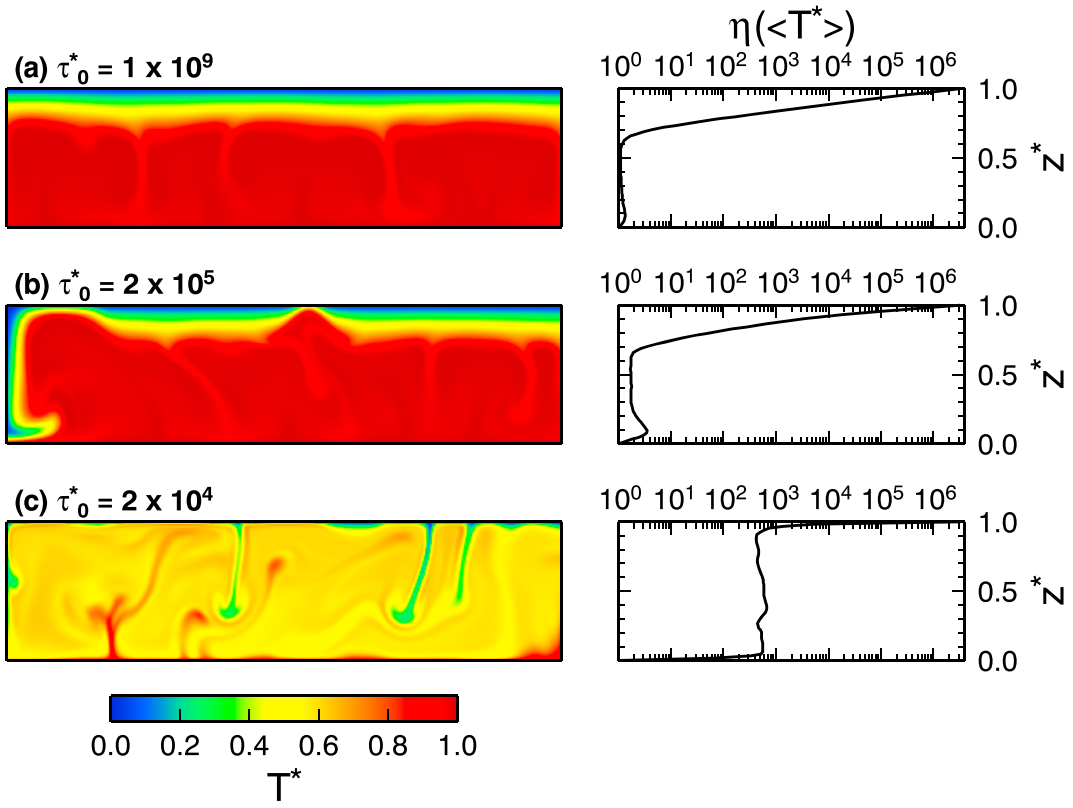

Figure 3. Three different convection regimes simulated with pseudoplastic rheology. (a) Stagnant lid convection with $\tau_0^* = 1 \times 10^9$. (b) Episodic overturn with $\tau_0^* = 2 \times 10^5$. (c) Mobile lid with $\tau_0^* = 2 \times 10^4$. All cases are with $Ra = 10^7$, $\theta = 15$, and $H^* = 3$. Left panels show temperature snapshots of statistically steady state solutions, and right panels show the temperature-dependent part of the rheology, calculated with the horizontally averaged temperature.

observations suggest that the Earth's upper mantle has cooled by only ~300 K over the last three billion years [*Herzberg et al.*, 2010].

2.3. Transient Solutions and the Urey Ratio

As mentioned in section 1, the mantle is heated both from within and from below, and its heating mode is fundamentally time dependent because the amount of radiogenic heating decreases steadily with time. However, statistically steady state solutions, such as those discussed in the previous section, are still useful because, even when the system is evolving, its characteristics at each time instant can be understood based on the scaling of such steady state solutions. In particular, when a system is cooling, the influence of secular cooling is thermally equivalent to an additional source of internal heating [e.g., *Daly*, 1980; *Christensen*, 1985b; *Weinstein and Olson*, 1990; *DeLandro-Clarke and Jarvis*, 1997; *Choblet and Sotin*, 2000]. It is critical to understand this issue when relating convection simulations to the thermal evolution of the Earth, yet there exist a fair number of recent studies that do not recognize the role of secular cooling. In this section, I use two simple examples to elucidate the crux of the transient heating mode. For simplicity, the bottom boundary is insulating in both examples, and I will focus on how transient solutions can be explained by the scaling of steady state solutions with purely internal heating.

For purely internal heating, *Solomatov and Moresi* [2000] derived the following heat flow scaling for (statistically steady state) stagnant lid convection with linear exponential rheology:

$$\left(1 - 2Nu^{-1} + 2a_{\mathrm{rh}}\theta^{-1}\right)^{1/2} = a\theta^{-(1+\beta)} Ra_s^{\beta} \exp(\beta\theta/Nu), \tag{17}$$

where $a_{\mathrm{rh}} = 2.4$, $\beta = 1/3$, and $a = 0.53$. Using equations (7), (8) and (16), and noting that *Solomatov and Moresi* [2000] normalize temperature with ΔT_H, the above scaling may be rearranged (see Appendix A) so that the surface heat flux is expressed as a function of internal parameters only:

$$q_t^* = T_i^* \left(1 - a_{\mathrm{rh}}\theta_i^{-1} + \left[\left(1 - a_{\mathrm{rh}}\theta_i^{-1}\right)^2 + a^2\theta_i^{-2(1+\beta)} Ra_i^{2\beta}\right]^{1/2}\right), \tag{18}$$

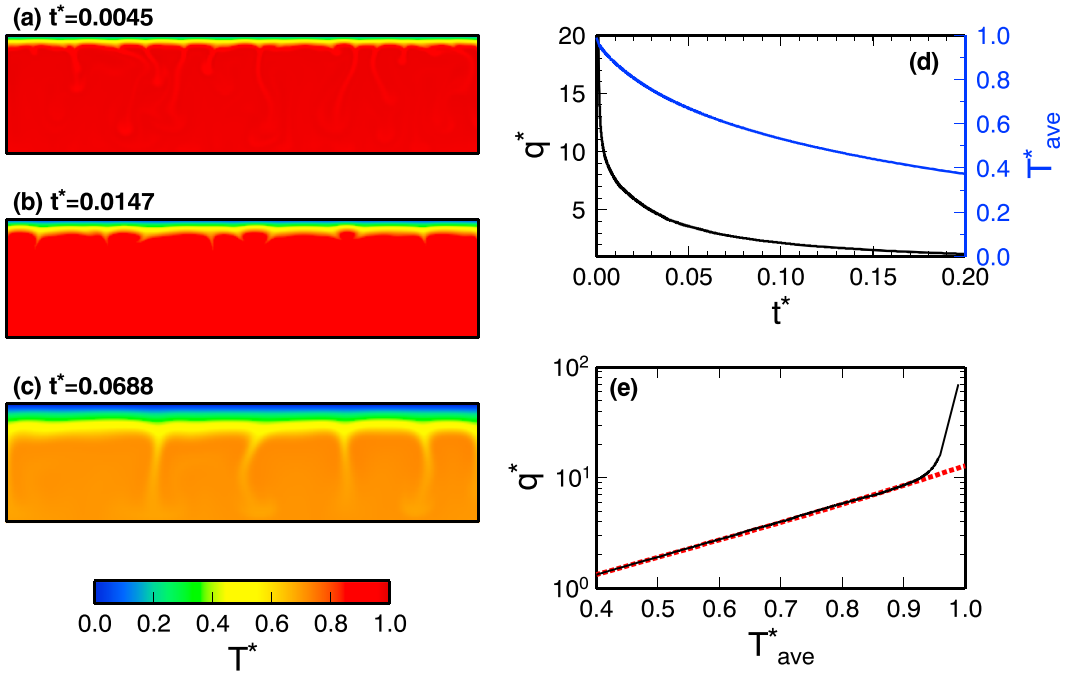

Figure 4. Instantaneous cooling simulation from a uniformly hot fluid ($T^*=1$) at $t^*=0$, with strongly temperature-dependent viscosity [θ=15 ($\Delta\eta \sim 3.3\times10^6$)]. The Rayleigh number is set to 3×10^8, the bottom boundary is insulating, and there is no internal heating. (a–c) Temperature snapshots at the time instants indicated. (d) Surface heat flux (black) and average internal temperature (blue) as a function of time. (e) Covariation of surface heat flux and average temperature (solid) is compared with the steady state scaling of *Solomatov and Moresi* [2000] (red dotted) (equations (18) and (19)).

where $\theta_i = \theta T_i^*$, and temperature is normalized by ΔT. This scaling is based on the internal temperature T_i^*, but it can be shown (see Appendix B) that the average temperature, which includes the contribution from the cold boundary layer, is related to the internal temperature as

$$\frac{T^*_{\text{ave}}}{T^*_i} = \frac{1-\delta+\delta^2/3}{1-\delta/2}, \tag{19}$$

where δ is the nondimensional thickness of the stagnant lid, which is given by $1-\sqrt{1-2/Nu}$.

In the first example, an initially uniformly hot fluid (with $T^*=1$) is cooled down from the top (Figure 4). The model setting is nearly identical to those shown in Figures 1g and 1i, with the insulating bottom boundary, θ=15 ($\Delta\eta \sim 3.3\times10^6$), and Ra=3×10^8. The only difference is that there is no internal heating, i.e., $H^*=0$, so the system is simply cooling down with time (Figure 4d). Each snapshot, however, looks very similar to steady state solutions for stagnant lid convection with purely internal heating, and indeed, the relation between surface heat flux and average temperature follows very closely the steady state scaling [equation (18)] (Figure 4e). The deviation from the scaling is seen when surface heat flux is greater than ~10, which corresponds to the initial phase in which heat is transported mostly by conduction. As soon as the system starts to convect vigorously, it follows the steady state scaling for purely internal heating. There is no internal heating in this instantaneous cooling simulation, so all of surface heat flux originates in secular cooling. In other words, secular cooling serves as effective internal heating.

The Urey ratio measures the contribution of radiogenic heat production to surface heat flux [*Christensen*, 1985a] and is given by

$$\text{Ur} = \frac{H^*}{q^*_t}. \tag{20}$$

In the instantaneous cooling simulation shown in Figure 4, the Urey ratio is always 0 because $H^*=0$, whereas the internal heating ratio ξ, if calculated at each time instant, would always be unity. When a system is cooling, the relation between the (instantaneous) heating mode and the amount of radiogenic internal heating becomes less obvious because of secular cooling.

The Earth's mantle always contains some amount of radioactive isotopes. As a slightly more realistic example, consider next a system in which internal heating decays as

$$H^*(t^*) = H_0^* \exp(-\lambda^* t^*) = H_0^* \exp(-t'), \tag{21}$$

where λ^* is the nondimensional decay constant and t' is the reduced time defined as $\lambda^* t^*$. One reduced time corresponds to the e-folding timescale for internal heat production. When the total surface heat flow is greater than the total internal heat production, a system should cool down, which in turn reduces surface heat flux (at least for the case of stagnant lid convection with no basal heating as considered here). But internal heating is also decreasing, and how closely surface heat flux can follow internal heating depends on how sensitive the heat flux is to changes in internal temperature [*Tozer*, 1972]. To quantify this, *Korenaga* [2016] introduced the Tozer number, which is defined as

$$Tz = \frac{\mathrm{d}q^*}{\mathrm{d}T^*_{\mathrm{ave}}} \frac{1}{\lambda^*}. \tag{22}$$

A system with a higher Tozer number (>1) can achieve a thermal equilibrium more easily.

For the second example, the steady state solution shown in Figure 1i is used as the initial condition. The initial internal heat production H_0^* is 6, and the average temperature is initially ~0.8. According to the heat flow scaling of *Solomatov and Moresi* [2000], $\mathrm{d}q^*/\mathrm{d}T^*_{\mathrm{ave}}$ is ~17 around this temperature for Ra of 3×10^8 and θ of 15. Figure 5 compares four cases with different Tozer numbers. When the Tozer number is as high as 30 (corresponding to very slowly decaying heat production), surface heat flux follows very closely the decaying internal heat production, but as the Tozer number decreases, the system moves away from such a thermal equilibrium (Figure 5a). In the absence of bottom heat flux, it can be shown that, when $Tz > 1$, the Urey ratio converges to $1 - Tz^{-1}$, and when $Tz \leq 1$, it converges to 0 [*Korenaga*, 2016]. The numerical results are consistent with this theoretical prediction (Figure 5b). Again, because the bottom boundary is insulating, the instantaneous internal heating ratio is always unity, but a range of the Urey ratio is possible. There is no unique relation between surface heat flux and internal heat production. Doubling internal heat production, for example, does not necessarily lead to doubling surface heat flux, though such an expectation is not uncommon in the literature [e.g., *Rüpke et al.*, 2004; *Hopkins et al.*, 2008]. Likewise, there is no unique relation between internal temperature and internal heat generation. The internal temperature at any time depends on the history of energy balance up to that point (Figure 5c). There exists, however, a simple relation between internal temperature and surface heat flux; as seen in Figure 5d, all cases considered fall on the steady state scaling for purely internal heating (equation (18)).

2.4. Connection to Geochemistry

Most of radiogenic heating in the mantle is provided by the decay of ^{235}U, ^{238}U, ^{232}Th, and ^{40}K, and geodynamical studies often rely on the geochemical literature for a reasonable range of radiogenic heat production. Certain conventions in geochemistry, however, may not be transparent to geophysicists, and as a result, geochemical constraints on heat production are sometimes quoted incorrectly, with nontrivial consequences. Thus, essential jargon related to this issue will be explained first in the following.

Figure 6a depicts genetic relations among conceptual geochemical Earth models. In geochemistry, it is common to assume that the bulk composition of the Earth is identical to, or very close to, that of carbonaceous chondrites, except for volatile elements, which could have been lost to space during high-energy planetary accretion processes. The primordial Earth is a hypothetical Earth in which no chemical differentiation has taken place. Core differentiation decomposes the primordial Earth into the primitive mantle and the core. The primitive mantle is also called the bulk silicate Earth and is parental to all silicate reservoirs in the present-day Earth. The chemical composition of the primitive mantle has been estimated by a variety of methods [e.g., *Jagoutz et al.*, 1979; *Hart and Zindler*, 1986; *McDonough and Sun*, 1995; *Allegre et al.*, 2001; *Palme and O'Neill*, 2003; *Lyubetskaya and Korenaga*, 2007a; *Korenaga*, 2009b], though many of them share similar assumptions. The concentration of heat-producing isotopes in the primitive mantle is higher than that in the primordial Earth by ~2, because those isotopes are mostly partitioned into the silicate mantle during core differentiation. Note that potassium is a volatile element, and its concentration in the primordial Earth is likely to be much lower than that in carbonaceous chondrites. The primitive mantle is a hypothetical concept and is not required to exist at any time in the Earth history. A certain amount of crustal material has probably existed all

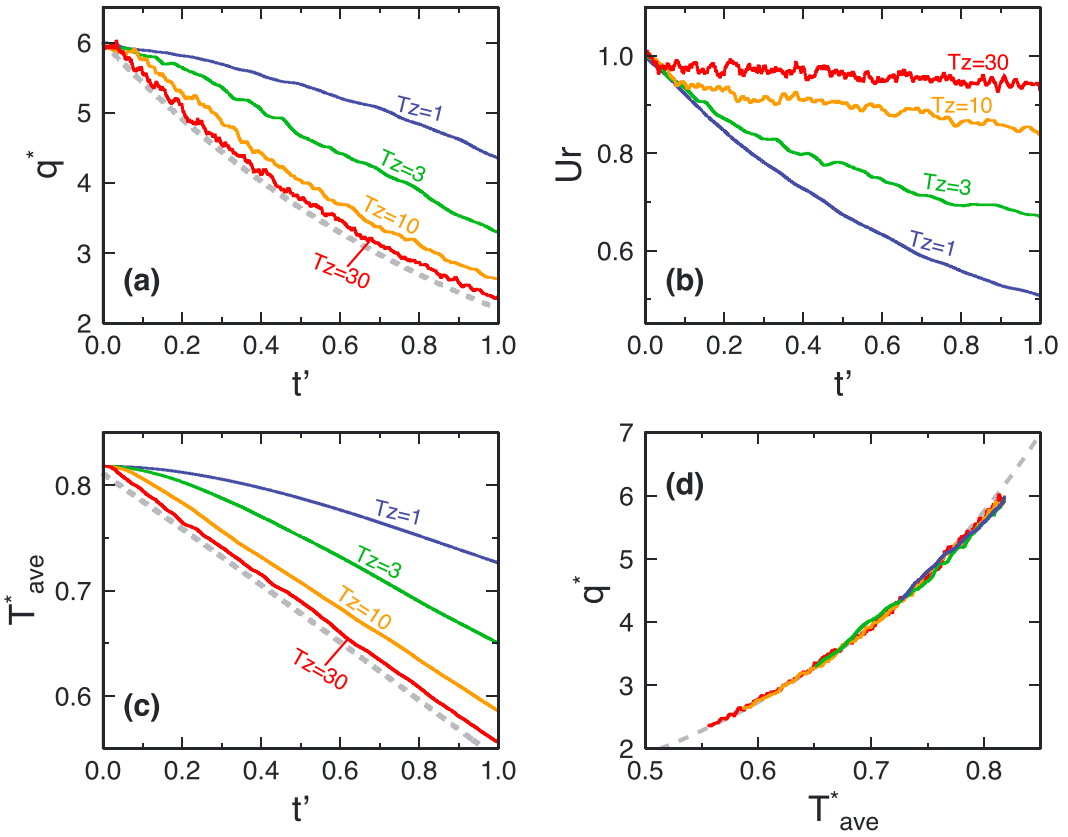

Figure 5. Summary of convection simulations with decaying heat production. The initial temperature field is taken from the steady state solution shown in Figure 1i. The Rayleigh number Ra is 3×10^8, the Frank-Kamenetskii parameter θ is 15 ($\Delta\eta \sim 3.3 \times 10^6$), and the bottom boundary is insulating. The heat production follows equation (21) with H_0^* of 6 (dashed curve in Figure 5a). (a) Surface heat flux, (b) Urey ratio, and (c) average internal temperature are shown as a function of the reduced time t'. Four values of the Tozer number are tested: 1 (blue), 3 (green), 10 (orange), and 30 (red). (d) The relation between the average temperature and heat flux. Gray dashed curve in Figure 5d is the steady state scaling of *Solomatov and Moresi* [2000] (equations (18) and (19)). Gray dashed curve in Figure 5c is the equilibrium average temperature corresponding to the heat flux based on this scaling. What is varied among these four cases is the decay constant λ^*, which is calculated as $(dq^*/dT^*_{ave})/Tz$ (equation (22)) with dq^*/dT^*_{ave} of 17 (an average value over the temperature range of ~ 0.7–0.8); for the case of Tz of 10, for example, λ^* is set to 1.7. Because the steady state heat flow scaling is not linear, dq^*/dT^*_{ave} varies around this assumed value as T^*_{ave} evolves, so the actual Tozer number of each case also deviates slightly from the value used to calculate λ^*.

the time, but the concept of the primitive mantle is useful when considering the silicate component of the Earth as a whole.

Crust-mantle differentiation throughout the Earth history has resulted in the present-day Earth, in which the primitive mantle is decomposed into the depleted mantle and the continental crust (Figure 6a). The continental crust is highly enriched in trace elements including heat-producing isotopes, so the extraction of the continental crust from the primitive mantle has left a mantle that is more depleted in those trace elements. Note that in this framework of global crust-mantle differentiation, the oceanic crust is usually considered as part of the depleted mantle, as subduction continuously recycles the oceanic crust into the mantle.

The depleted mantle represents the present-day convecting mantle as a whole, but geochemical data indicate that the mantle is compositionally highly heterogeneous [e.g., *Zindler and Hart*, 1986; *Hofmann*, 1997; *van Keken et al.*, 2002], and one popular notion is that the present-day mantle is divided into at least two layers (Figure 6a); the shallow and deep layers serve as sources for, respectively, mid-ocean ridge basalt (MORB) and ocean-island basalt (OIB). The MORB source mantle is generally more depleted in trace elements than the OIB source mantle. Table 1 lists several composition models and corresponding heat generation rates.

Under the assumption that the Earth is made from chondritic materials, the total amount of heat-producing isotopes in the whole Earth stays "chondritic" throughout internal differentiation processes. Once we decide

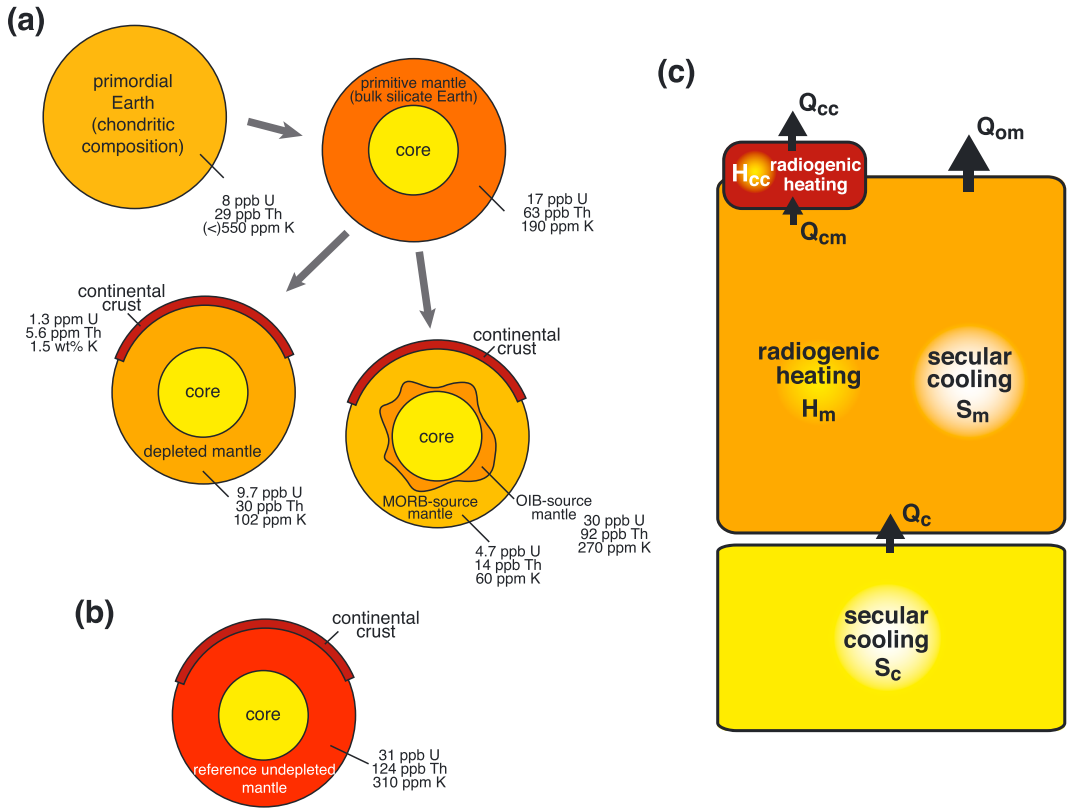

Figure 6. (a) Earth evolution through chemical differentiations. The primordial Earth evolves to the primitive mantle and the core upon core segregation, and the primitive mantle further evolves to the continental crust and the depleted mantle by crust-mantle differentiation. The depleted mantle denotes the present-day convecting mantle as a whole, and it is often decomposed further into the MORB source mantle and the OIB source mantle. There are quite a few composition models, and the concentration of heat-producing elements shown here is just an example. The primordial Earth composition is taken from the CI chondrite composition of *McDonough and Sun* [1995], the primitive mantle composition from *Lyubetskaya and Korenaga* [2007a], the continental crust composition from *Rudnick and Gao* [2003], and the MORB source composition from *Salters and Stracke* [2004]. The OIB source composition is calculated by mass balance assuming that it occupies 20% of the mantle mass. All of these concentrations come with relatively large uncertainties, which are omitted here for simplicity. (b) Schematic representation of the present-day situation according to the model of *Turcotte and Schubert* [2014], to be compared with the geochemical models shown in Figure 6a. (c) Schematic drawing to denote various components in the thermal budget of the Earth. Q_{cc} is surface heat flow from continental regions, Q_{om} is surface heat flow from oceanic regions, Q_{cm} is heat flow from the subcontinental mantle, H_{cc} is heat production within the continental crust, H_m is heat production within the mantle, S_m is heat flow due to the secular cooling of the mantle, Q_c is core heat flow, and S_c is heat flow due to the secular cooling of the core (including the effect of inner core growth). The possible presence of heat-producing elements in the core is neglected here for simplicity.

on composition models for the primitive mantle and the continental crust, therefore, we can calculate the composition of the depleted mantle by simple mass balance. Also, the compositions and mass fractions of the MORB source mantle and the OIB source mantle are such that they should add up to the composition of the depleted mantle. On the other hand, it is difficult to justify using the radiogenic heat generation of the primitive mantle for the convecting mantle; a substantial fraction of the present-day continental mass existed during most of the Earth history [e.g., *Campbell*, 2003; *Harrison*, 2009], so such use of the primitive mantle is inconsistent with the chondritic assumption (see *Lyubetskaya and Korenaga* [2007b, section 3.4] for further discussion).

Table 1 includes a "geophysical" estimate by *Turcotte and Schubert* [2014], which they call the "reference undepleted mantle." This geophysical estimate has been in their textbook since its first edition [*Turcotte and Schubert*, 1982], and it has been referred to in a number of geodynamical studies. Because it is not compatible with any geochemical estimates, however, it requires some explanation. They started with the present-day surface heat flow of 44.3 TW, subtracted the contribution of heat production within the continental crust,

Table 1. Mantle Composition Models and Heat Production

Authors	Model	U (ppb)	Th (ppb)	K (ppm)	H (10^{-12} W kg^{-1})
McDonough and Sun [1995]	Primitive mantle	20.3	79.5	240	4.92
Lyubetskaya and Korenaga [2007a]	Primitive mantle	17.3	62.6	190	4.01
Turcotte and Schubert [2014]	"Reference undepleted mantle"	31	124	310	7.38
Salters and Stracke [2004]	MORB source mantle	4.7	13.7	60	1.03
Workman and Hart [2005]	MORB source mantle	3.2	7.9	50	0.69
This study[a]	Depleted mantle	9.7	30	102	2.09
This study[b]	OIB source mantle	30	92	270	6.31

[a]Based on mass balance using the primitive mantle composition of *Lyubetskaya and Korenaga* [2007a]; the continental crust with 1.3 ppm U, 5.6 ppm Th, and 1.5 wt % K [*Rudnick and Gao*, 2003]; and the continental crustal mass of 2.37×10^{22} kg.

[b]Based on the above mass balance with the additional assumption that the MORB source mantle of *Salters and Stracke* [2004] occupies 80% of the mantle mass.

which was assumed to be 7.4 TW, and obtained the convective heat flow of 36.9 TW. They further assumed that secular cooling contributed only 20% of the convective heat flow, so the present-day radiogenic heat generation should account for 29.5 TW. The geochemistry of a wide variety of igneous rocks indicates that the ratios of K/U and Th/U are relatively constant as 1×10^4 and 4, respectively [e.g., *Wasserburg et al.*, 1964; *Gale et al.*, 2013]. So if the U concentration in the mantle is 31 ppb, the K and Th concentrations would be 310 ppm and 124 ppb, respectively, and the mantle heat production would match 29.5 TW. This is how their model of reference undepleted mantle was derived. The estimate given by the first edition *Turcotte and Schubert* [1982] is slightly different because a different value was used for the total heat flow, but the overall logic is the same. Also, the description of mantle heat production in *Schubert et al.* [2001, section 4.1.5] is the same as that in *Turcotte and Schubert* [2014].

Their assumption that 80% of the present-day convective heat flow comes from current radiogenic heat production, i.e., Ur is 0.8 at present, is based on classical models for the thermal evolution of the Earth [e.g., *Schubert et al.*, 1980; *Davies*, 1980], the validity of which has become increasingly questionable [e.g., *Korenaga*, 2008a; *Bradley*, 2008; *Herzberg et al.*, 2010; *Padhi et al.*, 2012; *Condie et al.*, 2015] (see also section 3.1). When using the reference undepleted mantle model of *Turcotte and Schubert* [2014] ($H = 7.38 \times 10^{-12}$ W kg^{-1}) for the present-day convecting mantle, it should be understood that the assumed heat production is ~350% of what is considered reasonable by the geochemical community (i.e., $H = 2.09 \times 10^{-12}$ W kg^{-1} for the depleted mantle). The term "undepleted" in the reference undepleted mantle of *Turcotte and Schubert* [2014] is used to indicate that it refers to the source mantle before melting beneath mid-ocean ridges. That is, it is undepleted with respect to the extraction of oceanic crust. But the present-day convecting mantle is already depleted with respect to the extraction of continental crust, and the reference undepleted mantle of *Turcotte and Schubert* [2014] should be compared with the depleted mantle, not with the primitive mantle (compare Figures 6a and 6b).

Various components in the thermal budget of the Earth are illustrated in Figure 6c. The total surface heat flow is the sum of oceanic and continental contributions, i.e., $Q_{om} + Q_{cc}$. The continental heat flow is the combination of heat production within the continental crust, H_{cc}, and heat flow from the subcontinental mantle, Q_{cm}, i.e., $Q_{cc} = H_{cc} + Q_{cm}$. The total convective heat flow is given by $Q_{om} + Q_{cm}$. The present-day (instantaneous) internal heating ratio is

$$\xi = \frac{Q_{om} + Q_{cm} - Q_c}{Q_{om} + Q_{cm}} = \frac{H_m + S_m}{Q_{om} + Q_{cm}}, \tag{23}$$

where Q_c is core heat flow, H_m is radiogenic heating in the mantle, and S_m is the secular cooling of the mantle. All of these quantities represent the present-day values. The core heat flow originates in the secular cooling of the core, so $Q_c = S_c$. The present-day Urey ratio is given by

$$\mathrm{Ur} = \frac{H_m}{Q_{om} + Q_{cm}}. \tag{24}$$

The present-day convective heat flow, $Q_{om} + Q_{cm}$, is estimated to be ~38 TW [*Korenaga*, 2008b], and if we use the heat production of the depleted mantle listed in Table 1 (2.09×10^{-12} W kg^{-1}), H_m would be ~8.4 TW, so Ur ~ 0.22. On the other hand, using the present-day core heat flow of ~5–15 TW [*Lay et al.*, 2008], the internal heating ratio ξ would be 0.61–0.87. How much internal heating we need to use in convection simulations depends on a chosen modeling strategy. If we aim to use steady state solutions as snapshots for the present-day situation, internal heating should be sufficiently high so that the above internal heating ratio can be reproduced. The amount of internal heating used in such steady state modeling has nothing to do with the actual concentration of radioactive isotopes. However, if instead we are to model the temporal evolution of the mantle directly, it is better to have the amount of internal heating consistent with the geochemical models of mantle composition. When using geochemically consistent internal heating, it becomes particularly important to take into account the effect of model geometry, as discussed in the next section.

2.5. Convection in a Spherical Shell

All numerical examples shown so far are with the two-dimensional (2-D) Cartesian geometry. As far as the heating mode is concerned, there is no essential difference between 2-D and 3-D Cartesian cases, and what we have learned from these 2-D examples is equally applicable to 3-D Cartesian cases. Mantle convection, however, takes places in a spherical shell, and the spherical geometry has some important effects on convection with internal heating.

For convection in a spherical shell, the top heat flux is not the same as the bottom heat flux even when H^* is 0, because the area is greater for the top surface. The system is cooled more efficiently from the above, and even when viscosity is spatially uniform and heating is purely basal, the convection system does not exhibit a symmetric thermal structure [e.g., *Bercovici et al.*, 1989]. Note that equations (13) and (14) still hold if the heat fluxes are replaced with total heat flows from relevant surfaces and the heat production with the total heat production from the entire fluid.

With the same amount of internal heating and the same bottom Rayleigh number, convection in a spherical shell tends to result in a lower internal temperature than that in a Cartesian box [*O'Farrell and Lowman*, 2010]. If one tries to simulate the temporal evolution of the mantle using a geochemically acceptable amount of internal heating, therefore, using the spherical geometry becomes important. Even if the amount of internal heating is geochemically reasonable, modeling with the Cartesian geometry would lead to a higher internal heating ratio than that with the spherical geometry, because cooling from the above is more reduced in the former. To simulate the temporal evolution of the mantle with the Cartesian geometry, one has to scale down the amount of internal heating to emulate the spherical geometry, but how to scale down has been studied only for simple viscosity models: constant viscosity [*O'Farrell and Lowman*, 2010] and depth-dependent viscosity [*O'Farrell et al.*, 2013]. Emulating convection in a spherical shell with the Cartesian geometry thus remains a challenge for more realistic mantle rheology. One might as well opt for just modeling with the spherical geometry, but directly simulating the long-term evolution of the Earth using realistic mantle rheology is still computationally demanding for 3-D models, given that mantle convection in the early Earth is likely to be characterized by very high Rayleigh numbers (10^9–10^{11} [*Korenaga*, 2010a]).

We can also study the temporal evolution of the mantle from the perspective of global energy balance (e.g., section 3.1), and in this case, the effect of spherical geometry can be handled more easily. The thermal evolution of the mantle is controlled by the balance of surface heat flux, core heat flux, and internal heating. The surface heat flux is usually modeled as a function of internal temperature, for which a steady state heat flux scaling with purely internal heating (e.g., equation (18)) is commonly used [e.g., *Grasset and Parmentier*, 1998; *Fraeman and Korenaga*, 2010]. The core heat flux can be parameterized as a function of the temperature jump at the core-mantle boundary as well as the viscosity of the lowermost mantle [e.g., *Stevenson et al.*, 1983]. These parametrizations are equivalent to assuming that heat fluxes from the top and bottom boundaries are controlled solely by the local instability of relevant boundary layers [e.g., *Howard*, 1966], and when the Rayleigh number is high enough, i.e., the system is vigorously convecting, this assumption appears to be valid even with complex mantle rheology [e.g., *Korenaga*, 2009a, 2010a]. For high Rayleigh number convection, a boundary layer is substantially thinner than the whole system, so the effect of sphericity is limited for its instability, as the radius of curvature does not vary much across the boundary layer. The consideration of spherical geometry enters into the global energy balance only as different surface areas for the top and bottom boundaries; i.e., surface and core heat fluxes as parametrized above have to be multiplied with relevant surface areas to yield total surface and core heat flows. Thus, if the parameterization of surface heat flux

can be decoupled from that of core heat flux, scaling laws established with the Cartesian geometry and with purely internal heating are still useful. The degree of possible coupling between these heat fluxes, however, has not been systematically investigated, and future studies are warranted on this important issue.

3. On the Effects of Higher Heat Production in the Past

The amount of radiogenic heat production was higher in the past than at present, because the heat is produced by radioacive decay, which means a greater abundance of relevant radioactive isotopes in the past. Also, the Earth's interior was most likely hotter in the past, because there is not enough internal heating to fully compensate for surface heat loss (at least at present; section 2.4). A hotter interior in the past, however, does not necessarily require higher heat production in the past (section 2.3). Similarly, higher heat production does not necessarily indicate more vigorous convection, though such a causal relation may be intuitively appealing. To help the reader to better understand the materials so far covered in a geological context, I discuss the following two questions: (1) did higher heat production result in higher surface heat flow in the past? and (2) did higher heat production lead to lower convective stress in the past? Both questions are directly related to mantle convection with internal heat production, with important implications for the long-term evolution of the Earth.

3.1. Was Surface Heat Flow Higher in the Past?

As indicated in section 2.3, surface heat flux can be a function of internal temperature; that is, under certain conditions, surface heat flux can be uniquely specified for a given internal temperature (e.g., Figure 5d). No unique relation, however, can be expected between internal temperature and internal heat production and between surface heat flux and internal heat production. This has already been noted in section 2.3 but in a rather abstract manner using the Tozer number. Also, in the particular example shown in Figure 5a, surface heat flux q^* decreases steadily with time, for a range of the Tozer number. Despite the nonunique relation between internal heat production and surface heat flux, therefore, it may give an impression that surface heat flow on the Earth should nevertheless be higher in the past than at present.

The relation between surface heat flux and internal heating is not so straightforward as the simple example implies, and to illustrate this point, I discuss two contrasting models proposed for the thermal evolution of the Earth. Consider the global energy balance for the mantle [e.g., *Stevenson et al.*, 1983], which may be expressed as

$$C_{\mathrm{m}} \frac{\mathrm{d}T_p}{\mathrm{d}t} = H(t) - Q(t) + Q_{\mathrm{c}}(t), \tag{25}$$

where C_{m} is the heat capacity of the entire mantle, T_p is the potential temperature of the mantle, H is the total radiogenic heating in the convecting mantle, Q is the convective heat loss at the surface, and Q_{c} is the heat flow from the core. The Urey ratio is given by H/Q, and the internal heating ratio is by $(Q - Q_{\mathrm{c}})/Q$. The secular evolution of the mantle temperature may be calculated by integrating this equation backward in time, starting from the present. The mantle heat capacity C_{m} is 4.97×10^{27} J K^{-1} [*Stacey*, 1981], the present-day potential temperature $T_p(0)$ is ~1350°C [*Herzberg et al.*, 2007], and the present-day convective heat flow $Q(0)$ is ~38 TW [*Korenaga*, 2008b]. As mentioned in section 2.4, the present-day core heat flow is only broadly estimated as ~5–15 TW [*Lay et al.*, 2008], and there is no robust observational constraint on its temporal variation [e.g., *Smirnov et al.*, 2016]. It would be most self-consistent to solve equation (25) in conjunction with a similar equation for the core, but for the sake of simplicity, the core heat flow is assumed here to vary linearly from 15 TW at 4.5 Ga to 10 TW at present. Such a cooling history of the core is among plausible solutions for a more complete coupled core-mantle evolution model [*O'Rourke et al.*, 2017]. With $Q_{\mathrm{c}}(t)$ fixed this way, equation (25) can be solved by specifying how $H(t)$ and $Q(t)$ should vary with time. Calculating the evolution of $H(t)$ is straightforward once we decide on the abundance of heat-producing elements in the mantle. There is not much disagreement on the relative abundance of those elements (i.e., K/U and Th/U), thus on the relative temporal evolution of internal heating, $H(t)/H(0)$. The absolute abundance of heat-producing elements can be represented succinctly by the present Urey ratio, Ur(0) [$= H(0)/Q(0)$], and its geochemically acceptable value is ~0.2–0.3 (section 2.4; see also *Korenaga* [2008a]).

What remains is the surface heat flow $Q(t)$, which is usually calculated through the relation between convective heat flux and mantle temperature, i.e., $Q(T_p(t))$, and this relation, the so-called heat flux scaling, has been debated since the mid-1980s [e.g., *Christensen*, 1985a; *Gurnis*, 1989; *Solomatov*, 1995; *Conrad and Hager*, 1999;

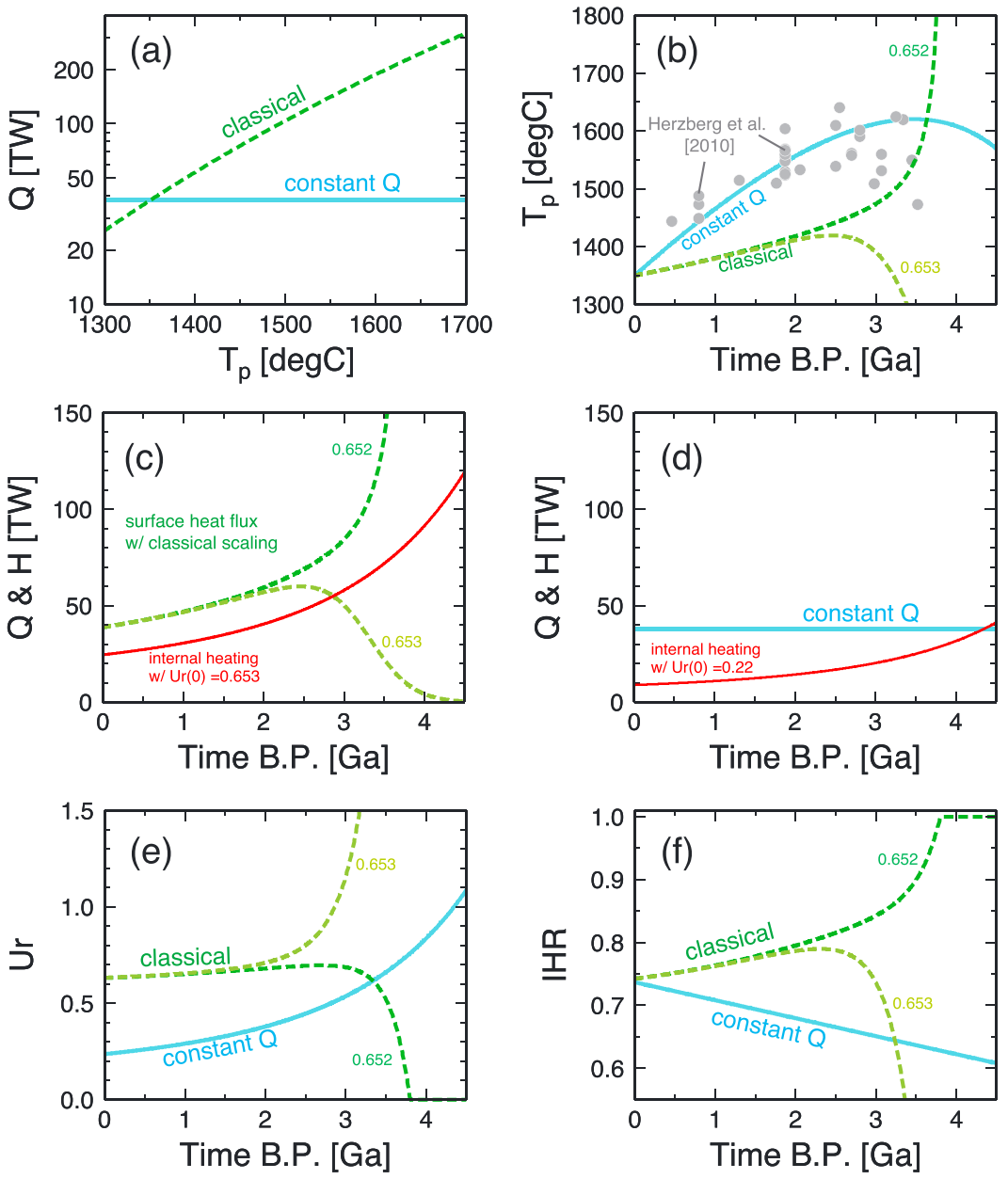

Figure 7. (a) Two heat flow scaling laws used for thermal evolution modeling: classical (dashed) and constant heat flow (solid). See *Korenaga* [2013] for further details. (b) The evolution of mantle potential temperature with constant heat flow and Ur(0) of 0.22 (solid) and with the classical scaling and Ur(0) of 0.652–0.653 (dashed). Solid circles denote petrological estimates on past potential temperature [*Herzberg et al.*, 2010]. B.P. denotes "before present." (c) The evolution of surface heat flow (green) and radiogenic heating (red) for the classical heat flow scaling. (d) Same as Figure 7c but for the constant heat flow scaling. (e) The evolution of Urey ratio. (f) The evolution of the internal heating ratio.

Korenaga, 2003, 2010a]. A hotter mantle in the past has long been assumed to convect more vigorously with higher surface heat flow [e.g., *Davies*, 1980; *Schubert et al.*, 2001], and such scaling is labeled as "classical" in Figure 7a. This scaling is based on the *Nu-Ra* relation of isoviscous convection, combined with the temperature dependence of mantle viscosity. One practical problem with this classical scaling is that it requires an excessive amount of radiogenic heat production in the mantle (Ur(0) $\sim$ 0.65), much more than implied by geochemistry, to reproduce a geologically reasonable thermal history (Figure 7b). If we use a geochemically reasonable value of $\sim$0.2–0.3 instead, the classical scaling is known to result in a highly divergent solution widely referred to as the "thermal catastrophe" case [*Christensen*, 1985a] (see *Korenaga* [2013, section 2.3] for a brief summary

on this issue). Also, thermal evolution modeling with the classical scaling is known to exhibit an extreme sensitivity to the assumed value of Ur(0) (compare curves labeled 0.652 and 0.653 in Figure 7b). The origin of this sensitivity can be traced to the "self-regulation" or high Tozer number achieved by the classical scaling [*Tozer*, 1972; *Korenaga*, 2016]. With an increasing Tozer number, the system evolution becomes more independent of its initial state, so a wide range of initial states can converge to an identical present-day state. When integrating the energy balance equation backward in time, this convergence forward in time emerges as divergence backward in time.

In contrast, if one considers the effect of melting beneath mid-ocean ridges on mantle viscosity, a hotter mantle does not necessarily convect faster, and the surface heat flow could become virtually insensitive to the internal temperature [*Korenaga*, 2003, 2011]. This possibility is represented by the constant heat flux scaling in Figure 7a. The virtue of this scaling is that it can reproduce a reasonable thermal history without violating geochemical constraints, and furthermore, a reconstructed thermal history is consistent with the cooling history of the upper mantle inferred from igneous petrology [*Herzberg et al.*, 2010] (Figure 7b). The high Urey ratio that is required for the use of classical scaling means a minor role of secular cooling, so high Urey ratio models are generally unable to reproduce the cooling rate of $\sim$100 K Gyr^{-1} as suggested by *Herzberg et al.* [2010].

Even in the classical model, surface heat flow is not always higher in the past; its temporal variation is very sensitive to the assumption on the amount of internal heat production (Figure 7c). In the model of the constant heat flow, surface heat flow in the past is identical to the present-day value by assumption (Figure 7d). However, because this model is consistent with the secular cooling trend as well as the geochemical budget on internal heat production, it may also be said that surface heat flow in the past should not be very different from the present-day value in order to satisfy these observational constraints.

The evolution of the Urey ratio is shown in Figure 7e and that of the internal heating ratio in Figure 7f, for both of these two models. For the classical model, the temporal behaviors of the Urey ratio and the internal heating ratio are similar; they are nearly constant before divergence at $\sim$3 Ga. For the constant heat flow model, however, their behaviors are opposite; the Urey ratio is higher in the past because radiogenic heat production was higher, but the internal heating ratio is lower in the past because effective heat production including secular cooling is lower.

3.2. Was Convective Stress Lower in the Past?

As indicated in the previous section, higher internal heating does not always result in higher heat flow for two reasons: (1) higher internal heating does not guarantee higher internal temperature (Figure 7b), and (2) higher internal temperature does not necessarily mean higher heat flow (Figure 7a; note that the constant heat flow scaling is a good approximation to a more realistic scaling with the effect of water on the evolution of mantle viscosity [*Korenaga*, 2011]). Whereas the first statement is a simple consequence of global energy balance, the second one entails a long-standing debate over the heat flux scaling of mantle convection. As far as the thermal evolution of the Earth is concerned, this debate has long been about the scaling of plate tectonics, because the thermal history of the Earth is commonly studied with a single heat flux scaling $Q(T_p)$. The use of just one scaling is equivalent to assuming that plate tectonics has been in operation for the duration under consideration (e.g., 4.5 Gyr in Figure 7). This is, however, an unwarranted assumption, given that the onset of plate tectonics in the Earth history has been hotly debated in recent years [e.g., *Condie and Kröner*, 2008; *Korenaga*, 2013]. The mode of mantle convection may have been different in the past [e.g., *Stern*, 2005; *O'Neill et al.*, 2007; *Silver and Behn*, 2008; *Arndt and Davaille*, 2013], and this is one of the outstanding problems in mantle dynamics, with a close connection to exoplanetary research [e.g., *Valencia et al.*, 2007; *O'Neill and Lenardic*, 2007; *Korenaga*, 2010b; *van Heck and Tackley*, 2011]. It is also a difficult problem to tackle, involving complex mantle rheology, the sensitivity to initial conditions, and time-varying boundary conditions [e.g., *Stein et al.*, 2013; *Weller et al.*, 2015; *O'Neill et al.*, 2016], most of which are still poorly understood. Considering such a multitude of controlling factors, it is desirable to have a clear understanding of elementary processes, as it may help us to better interpret the outcome of complex models. In this spirit, I take a close look at one particularly popular notion among these studies: Higher internal production results in lower convective stress and thus tends to prevent the operation of plate tectonics [e.g., *Stein et al.*, 2004; *O'Neill et al.*, 2007; *Stein et al.*, 2013; *Weller et al.*, 2015].

The study of *Stein et al.* [2004] was the first to investigate the influence of internal heating on the mode of convection, and a physical explanation for this influence was sought by *O'Neill et al.* [2007], using numerical simulations of stagnant lid convection. *O'Neill et al.* [2007] found that convective stress, which is reflected

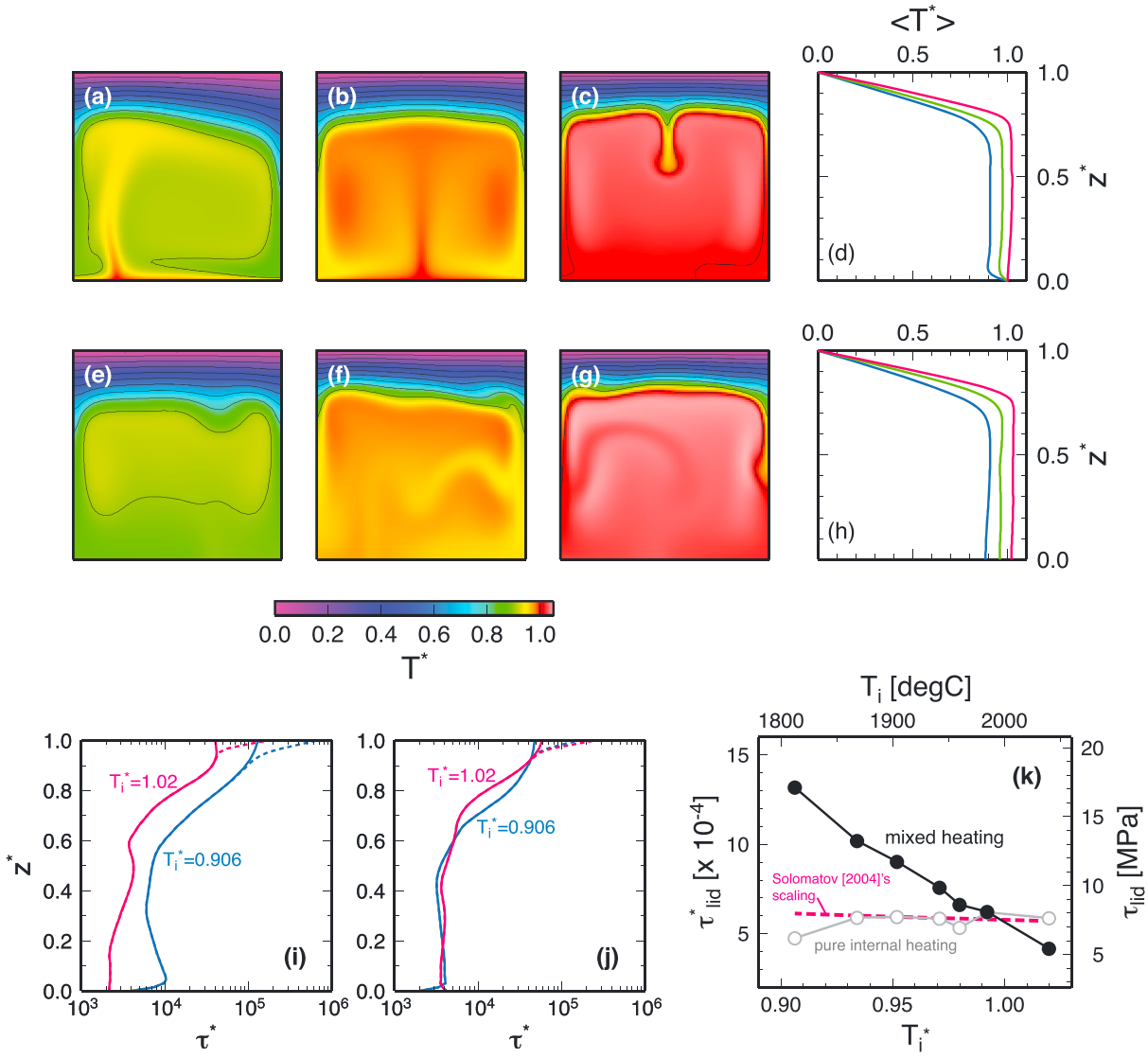

Figure 8. Temperature snapshots of stagnant lid simulation with the total viscosity contrast of 10^5 and the bottom Rayleigh number of 10^7 and with internal heating of (a) 0, (b) 1.5×10^{-11} W kg^{-1} ($H^* = 2.78$), and (c) 3×10^{-11} W kg^{-1} ($H^* = 5.56$). (d) Horizontally averaged temperature profiles for these three cases, $H = 0$ (blue), $H = 1.5 \times 10^{-11}$ W kg^{-1} (green), and $H = 3 \times 10^{-11}$ W kg^{-1} (red). (e–g) Snapshots of stagnant lid convection with purely internal heating (i.e., with an insulated bottom). The amount of internal heating is adjusted so that each case reproduces the internal temperature (and also the internal Rayleigh number) of the case shown above, which may be verified by comparing Figures 8d and 8h. Horizontally averaged stress profiles are shown (i) for the cases of Figures 8a (blue) and 8c (red), and (j) for the cases of Figures 8e (blue) and 8g (red). Solid and dashed curves denote, respectively, results with rigid and free-slip boundary conditions, and the one with rigid boundary condition is most relevant to the yielding of lithosphere [*Solomatov*, 2004]. (k) Maximum lid stress as a function of internal temperature for the cases of the fixed bottom temperature (solid circles) and the insulated bottom (open circles). Note that internal temperature, as opposed to internal heating, has to be used here to compare these two cases. Dashed line denotes prediction based on the stress scaling of *Solomatov* [2004], which is applicable to convection with purely internal heating. The stress prediction is not accurate enough to match the amplitude of numerical results, and a factor of 1/3 is multiplied here.

in lithospheric stress, decreased as internal heating increased, and they reasoned as follows. With greater internal heating, the mantle is hotter, and mantle viscosity is lower. Even though a hotter mantle convects more vigorously, the effect of lower viscosity dominates, resulting in a negative correlation between internal heating and convective stress. A set of stagnant lid simulations conducted by *O'Neill et al.* [2007] are reproduced in Figures 8a–8d. Here the top and bottom boundaries used free-slip conditions. A temperature scale ΔT of 2000 K was used, and the normalized temperature was fixed to 0 at the top and 1 at the bottom. The Frank-Kamenetskii parameter θ was 11.5 ($\Delta\eta \sim 10^5$). The bottom Rayleigh number was set to 10^7 for all simulations. All models were run long enough to reach a statistically steady state. Lithospheric stress indeed decreases with increasing heat production (Figure 8k; cf. Figure 3 of *O'Neill et al.* [2007]).

It can also be seen, however, that the heating mode varies from purely basal heating ($H = 0$) to virtually purely internal heating ($H = 3 \times 10^{-11}$ W kg^{-1}). As the internal temperature increases with higher internal heating, therefore, the bottom thermal boundary layer (and upwelling from it) also diminishes. To quantify the influence of the bottom boundary layer, I also constructed corresponding purely internal heating cases with the same internal temperatures and the same internal Rayleigh numbers but without a bottom boundary layer (Figures 8e–8h). As seen in Figures 8i–8k, the strong dependence of convective stress on internal heating is caused mostly by variations in the bottom boundary layer; variations in the internal temperature have only minute influence on lithospheric stress, which is also consistent with the stress scaling of *Solomatov* [2004] (Figure 8k). A correct interpretation of the negative correlation between internal heating and convective stress would thus be the following: different heating modes, or varying contributions from the bottom boundary layer, could influence the magnitude of lithospheric stress.

To quantify the relative magnitude of convective stress in the past, therefore, we need to know how the heating mode of actual mantle convection has changed through time. It depends not only on internal heating of the mantle but also on other components of the global thermal budget, such as the secular evolution of surface heat flow and core heat flow. As indicated by the thermal evolution models considered in the previous section (Figure 7f), the internal heating ratio in the past is not necessarily higher than the present-day value. The case with the classical scaling shows that the ratio is higher in the past (at least back to ~2 Ga), and this is because the temporal variation of surface heat flow outweighs that of the assumed core heat flow. In contrast, the case with the constant heat flow scaling shows the opposite trend, because the surface heat flow is constant while the core heat flow is higher in the past. These temporal variations of the internal heating ratio can be modified by using different assumptions for core heat flow, but the following two points would likely remain valid. First, the degree of the increase seen with the classical scaling is only modest before the corresponding thermal evolution starts to diverge. Second, with the constant heat flow scaling, or more generally with low Urey ratio models, a higher internal heating ratio in the past is possible only when the core heat flow is lower in the past.

4. Concluding Remarks

The mantle of the Earth (and probably of other terrestrial planets as well) is heated from below and within. It may thus seem most appropriate to use mixed heating when modeling mantle convection, but doing it correctly is not a trivial task. In the following, the main points discussed in this paper are summarized as pitfalls, together with my suggestions for how to avoid them.

1. Using the realistic concentration of heat-producing elements for internal heating does not necessarily produce a realistic simulation of mantle convection, even with a spherical geometry. On the contrary, it will most likely fail to reproduce the heating mode of actual mantle convection if the simulation is run to obtain a steady state solution. For steady state solutions, the effect of secular cooling has to be taken into account as additional internal heating.
2. For transient solutions, using a geochemical estimate on radiogenic heat production, after properly scaled to an adopted model geometry, becomes important, although a clear understanding of the meaning of the different geochemical models is needed. A "chondritic" heat production by itself does not carry much information, because most geochemical models are based on the chondritic assumption. Using the primitive mantle model for the convecting mantle neglects that nearly half of the heat-producing elements in the Earth are contained presently in the continental crust. Also, note that using the reference undepleted mantle model of *Turcotte and Schubert* [2014] is equivalent to exceeding geochemical constraints by more than a factor of 3.
3. For mixed heating, it is still difficult to predict the internal temperature and the internal heating ratio a priori, so it is important to always measure them to see if simulation results meet expectations. This is especially true when conducting a series of simulations to understand the sensitivity of a certain convection diagnostic (e.g., average surface velocity and surface heat flux) to model parameters. When conducting a control experiment, one should aim to change only one variable at a time and bear in mind that changing one model parameter does not always change just one variable. Changing the amount of internal heat production while fixing all other model parameters, for example, usually leads to changing two variables, the internal temperature and the internal heating ratio.
4. With mixed heating, only a certain fraction of the total temperature scale is contained in the top boundary layer, so when using temperature-dependent viscosity, only a fraction of the total viscosity contrast is

represented by the top boundary layer. This viscosity contrast across the top boundary layer is most relevant to the strength of surface plates and thus important for the mode of mantle convection.

5. Different internal heating ratios imply that the relative importance of the top and bottom boundaries can vary among simulations. Boundary layer instabilities are what drives convection, so when reporting simulation results with mixed heating, it is important to include the internal heating ratio along with the internal temperature. Otherwise, it is difficult to evaluate the relevance of simulated convection to planetary evolution.
6. It is often advisable to start with simulations with purely internal heating and then investigate the effect of mixed heating using the cases of purely internal heating as a reference. Even with purely internal heating, it is still difficult to predict the internal temperature a priori when a complex viscosity function is employed, but purely internal heating is considerably easier to handle because the internal heating ratio is always unity and the top boundary layer carries all of the temperature and viscosity contrasts.
7. Not all simulation results with mixed heating can necessarily find their direct application to planetary evolution, because a realistic range of the internal heating ratio is determined by the thermal evolution of a planet. In particular, the thermal evolution of the Earth is a complex subject, requiring us to digest not only geodynamics but also geochemistry and geology, but it is essential to consider the physics of mantle convection within the framework of the transient Earth.

Appendix A: Derivation of Equation (18)

Equation (17) is based on the temperature scale of ΔT_H [*Solomatov and Moresi*, 2000], so $Nu = 1/T_i^*$, and $\exp(\theta)$ represents the total viscosity variation over the range of ΔT_H. The use of the surface Rayleigh number Ra_s in this equation is consistent with the adopted temperature scale. Equation (17) by itself is not easy to use because Nu appears inside the square root on the left-hand side and within the exponential function on the right-hand side. It can be rearranged to a more straightforward expression such as equation (18) as follows.

First, from equations (6)–(8), we have

$$\frac{Ra_s}{Ra_i} = \frac{\Delta T_H}{\Delta T T_i^*}\frac{\eta_i}{\eta_s} = Nu\ \exp(-\theta_i), \tag{A1}$$

where $\theta_i = \theta T_i^*$. Note that T_i^* in the above is from equation (8) and is normalized by ΔT. Thus, the term $\Delta T_H/(\Delta T T_i^*)$ as a whole is equivalent to $1/T_i^*$ (where T_i^* is normalized by ΔT_H), which is Nu. The quantity $\exp(\theta_i)$ corresponds to the relative viscosity variation between the surface temperature and the internal temperature, i.e., η_s/η_i. Second, $\exp(\beta\theta/Nu)$ in the right-hand side of equation (17) is equivalent to $\exp(\beta\theta_i)$ because $Nu = 1/T_i^*$. Then, using $\theta = \theta_i/T_i^* = \theta_i\, Nu$ and equation (A1), equation (17) may be expressed as

$$Nu\left[1 - 2Nu^{-1}\left(1 - a_{\mathrm{rh}}\theta_i^{-1}\right)\right]^{1/2} = a\theta_i^{-(1+\beta)}Ra_i^{\beta}, \tag{A2}$$

which can be solved for Nu as

$$Nu = 1 - a_{\mathrm{rh}}\theta_i^{-1} + \left[\left(1 - a_{\mathrm{rh}}\theta_i^{-1}\right)^2 + a^2\theta_i^{-2(1+\beta)}Ra_i^{2\beta}\right]^{1/2}. \tag{A3}$$

Equation (18) is derived from the above by noting that $Nu = q_t^*/T_i^*$ with the temperature scale of ΔT.

Appendix B: Derivation of Equation (19)

For a statistically steady state of stagnant lid convection with purely internal heating, the vertical profile of horizontally averaged temperature may be divided into two parts, a conductive lid and an isothermal convecting interior. With uniform internal heating, a conductive profile within the lid may be expressed as

$$T^* = z^* - \frac{1}{2}(z^*)^2, \tag{B1}$$

where temperature is normalized by ΔT_H, and z^* is 0 at the surface and increases downward. At the base of the lid, i.e., $z^* = \delta$, the temperature matches the internal temperature, so

$$T_i^* = \delta\left(1 - \frac{1}{2}\delta\right). \tag{B2}$$

Because $Nu = 1/T_i^*$, the above equation may be solved for the boundary layer thickness as

$$\delta = 1 - \sqrt{1 - 2/Nu}. \tag{B3}$$

The average temperature of the entire system is given by

$$T_{\mathrm{ave}}^* = \int_0^\delta \left(\zeta - \frac{1}{2}\zeta^2\right) \mathrm{d}\zeta + (1-\delta)T_i^* = \delta\left(1 - \delta + \frac{1}{3}\delta^2\right). \tag{B4}$$

Equation (19) is derived from equations (B2) and (B4). Note that equation (19) was incorrectly published in *Korenaga* [2016].

Acknowledgments
This material is based upon work supported by the U.S. National Aeronautics and Space Administration through the NASA Astrobiology Institute under Cooperative Agreement NNA15BB03A issued through the Science Mission Directorate. The author thanks Dave Bercovici, Michael Manga, Elvira Mulyukova, and Juan Rosas for constructive comments on the earlier version of the manuscript. The author also thanks Julian Lowman, an anonymous reviewer, and the Associate Editor for thoughtful reviews, which helped to improve substantially the clarity and accuracy of the manuscript. This work is theoretical in nature, and no specific data sources were used outside of works cited.

References

Allegre, C., G. Manhes, and E. Lewin (2001), Chemical composition of the Earth and the volatility control on planetary genetics, *Earth Planet. Sci. Lett.*, *185*, 49–69.
Arndt, N., and A. Davaille (2013), Episodic Earth evolution, *Tectonophysics*, *609*, 661–674.
Bercovici, D., G. Schubert, G. A. Glatzmaier, and A. Zebib (1989), Three-dimensional thermal convection in a spherical shell, *J. Fluid Mech.*, *206*, 75–104.
Bercovici, D., Y. Ricard, and M. A. Richards (2000), The relation between mantle dynamics and plate tectonics: A primer, in *The History and Dynamics of Global Plate Motions*, edited by M. A. Richards, R. G. Gordon, and R. D. van der Hilst, pp. 5–46, AGU, Washington, D. C.
Bradley, D. C. (2008), Passive margins through Earth history, *Earth Sci. Rev.*, *91*, 1–26.
Campbell, I. H. (2003), Constraints on continental growth models from Nb/U ratios in the 3.5 Ga Barberton and other Archaean basalt-komatiite suites, *Am. J. Sci.*, *303*, 319–351.
Choblet, G. (2012), On the scaling of heat transfer for mixed heating convection in a spherical shell, *Phys. Earth Planet. Inter.*, *206–207*, 31–42.
Choblet, G., and E. Parmentier (2009), Thermal convection heated both volumetrically and from below: Implications for predictions of planetary evolution, *Phys. Earth Planet. Inter.*, *173*, 290–296.
Choblet, G., and C. Sotin (2000), 3D thermal convection with variable viscosity: Can transient cooling be described by a quasi-static scaling law?, *Phys. Earth Planet. Inter.*, *119*, 321–336.
Christensen, U. R. (1985a), Thermal evolution models for the Earth, *J. Geophys. Res.*, *90*, 2995–3007.
Christensen, U. R. (1985b), Heat transport by variable viscosity convection II: Pressure influence, non-Newtonian rheology and decaying heat sources, *Phys. Earth Planet. Inter.*, *37*, 183–205.
Christensen, U. R. (1989), Mantle rheology, constitution, and convection, in *Mantle Convection: Plate Tectonics and Global Dynamics*, edited by W. R. Peltier, pp. 595–655, Gordon and Breach Science Publ., New York.
Condie, K., S. Pisarevsky, J. Korenaga, and S. Gardoll (2015), Is the rate of supercontinent assembly changing with time?, *Precambrian Res.*, *259*, 278–289.
Condie, K. C., and A. Kröner (2008), When did plate tectonics begin? Evidence from the geologic record, in *When Did Plate Tectonics Begin on Planet Earth?*, edited by K. C. Condie and V. Pease, pp. 281–294, Geol. Soc. Am., Boulder, Colo.
Conrad, C. P., and B. H. Hager (1999), The thermal evolution of an Earth with strong subduction zones, *Geophys. Res. Lett.*, *26*, 3041–3044.
Daly, S. F. (1980), Convection with decaying heat sources: Constant viscosity, *Geophys. J. R. Astron. Soc.*, *61*, 519–547.
Davies, G. F. (1980), Thermal histories of convective Earth models and constraints on radiogenic heat production in the Earth, *J. Geophys. Res.*, *85*, 2517–2530.
DeLandro-Clarke, W., and G. T. Jarvis (1997), Numerical models of mantle convection with secular cooling, *Geophys. J. Int.*, *129*, 183–193.
Deschamps, F., and J.-R. Lin (2014), Stagnant lid convection in 3D-Cartesian geometry: Scaling laws and applications to icy moons and dwarf planets, *Phys. Earth Planet. Inter.*, *229*, 40–54.
Deschamps, F., P. J. Tackley, and T. Nakagawa (2010), Temperature and heat flux scalings for isoviscous thermal convection in spherical geometry, *Geophys. J. Int.*, *182*, 137–154.
Fleitout, L., and D. A. Yuen (1984), Steady state, secondary convection beneath lithospheric plates with temperature- and pressure-dependent viscosity, *J. Geophys. Res.*, *89*, 9227–9244.
Foley, B. J., and D. Bercovici (2014), Scaling laws for convection with temperature-dependent viscosity and grain-damage, *Geophys. J. Int.*, *199*, 580–603.
Fraeman, A. A., and J. Korenaga (2010), The influence of mantle melting on the evolution of Mars, *Icarus*, *210*, 43–57.
Gale, A., C. A. Dalton, C. H. Langmuir, Y. Su, and J.-G. Schilling (2013), The mean composition of ocean ridge basalts, *Geochem. Geophys. Geosyst.*, *14*, 489–518, doi:10.1029/2012GC004334.
Grasset, O., and E. Parmentier (1998), Thermal convection in a volumetrically heated, infinite Prandtl number fluid with strongly temperature-dependent viscosity: Implications for planetary thermal evolution, *J. Geophys. Res.*, *103*, 18,171–18,181.
Gurnis, M. (1989), A reassessment of the heat transport by variable viscosity convection with plates and lids, *Geophys. Res. Lett.*, *16*, 179–182.
Harrison, T. M (2009), The Hadean crust: Evidence from >4 Ga zircons, *Annu. Rev. Earth Planet. Sci.*, *37*, 479–505.
Hart, S. R., and A. Zindler (1986), Search of a bulk-Earth composition, *Chem. Geol.*, *57*, 247–267.
Herzberg, C., P. D. Asimow, N. Arndt, Y. Niu, C. M. Lesher, J. G. Fitton, M. J. Cheadle, and A. D. Saunders (2007), Temperatures in ambient mantle and plumes: Constraints from basalts, picrites, and komatiites, *Geochem. Geophys. Geosyst.*, *8*, Q02206, doi:10.1029/2006GC001390.
Herzberg, C., K. Condie, and J. Korenaga (2010), Thermal evolution of the Earth and its petrological expression, *Earth Planet. Sci. Lett.*, *292*, 79–88.
Hofmann, A. W. (1997), Mantle geochemistry: The message from oceanic volcanism, *Nature*, *385*, 219–229.
Hopkins, M., T. M. Harrison, and C. E. Manning (2008), Low heat flow inferred from >4 Gyr zircons suggest Hadean plate boundary interactions, *Nature*, *456*, 493–496.
Howard, L. N. (1966), Convection at high Rayleigh number, in *Proceedings of the 11th International Congress of Applied Mechanics*, edited by H. Gortler, pp. 1109–1115, Springer, New York.

Jagoutz, E., H. Palme, H. Baddenhausen, K. Blum, M. Cendales, G. Dreibus, B. Spettel, V. Lorenz, and H. Wanke (1979), The abundances of major, minor and trace elements in the Earth's mantle as derived from primitive ultramafic nodules, in *Proceedings of the 10th Lunar Planetary Science Conference*, edited by R. B. Merrill et al., pp. 2031–2050, Pergamon Press, New York.
Karato, S., and P. Wu (1993), Rheology of the upper mantle: A synthesis, *Science*, *260*, 771–778.
Korenaga, J. (2003), Energetics of mantle convection and the fate of fossil heat, *Geophys. Res. Lett.*, *30*, 1437, doi:10.1029/2003GL016982.
Korenaga, J. (2008a), Urey ratio and the structure and evolution of Earth's mantle, *Rev. Geophys.*, *46*, RG2007, doi:10.1029/2007RG000241.
Korenaga, J. (2008b), Plate tectonics, flood basalts, and the evolution of Earth's oceans, *Terra Nova*, *20*, 419–439.
Korenaga, J. (2009a), Scaling of stagnant-lid convection with Arrhenius rheology and the effects of mantle melting, *Geophys. J. Int.*, *179*, 154–170.
Korenaga, J. (2009b), A method to estimate the composition of the bulk silicate Earth in the presence of a hidden geochemical reservoir, *Geochim. Cosmochim. Acta*, *73*, 6952–6964.
Korenaga, J. (2010a), Scaling of plate-tectonic convection with pseudoplastic rheology, *J. Geophys. Res.*, *115*, B11405, doi:10.1029/2010JB007670.
Korenaga, J. (2010b), On the likelihood of plate tectonics on super-Earths: Does size matter?, *Astrophys. J. Lett.*, *725*, L43—L46.
Korenaga, J. (2011), Thermal evolution with a hydrating mantle and the initiation of plate tectonics in the early Earth, *J. Geophys. Res.*, *116*, B12403, doi:10.1029/2011JB008410.
Korenaga, J. (2013), Initiation and evolution of plate tectonics on Earth: Theories and observations, *Annu. Rev. Earth Planet. Sci.*, *41*, 117–151.
Korenaga, J. (2016), Can mantle convection be self-regulated?, *Sci. Adv.*, *2*, e1601168.
Korenaga, J., and T. H. Jordan (2003), Physics of multiscale convection in Earth's mantle: Onset of sublithospheric convection, *J. Geophys. Res.*, *108*, 2333, doi:10.1029/2002JB001760.
Landuyt, W., and D. Bercovici (2009), Variations in planetary convection via the effect of climate on damage, *Earth Planet. Sci. Lett.*, *277*, 29–37.
Lay, T., J. Hernlund, and B. A. Buffett (2008), Core-mantle boundary heat flow, *Nat. Geosci.*, *1*, 25–32.
Lourenço, D. L., A. Rozel, and P. J. Tackley (2016), Melting-induced crustal production helps plate tectonics on Earth-like planets, *Earth Planet. Sci. Lett.*, *439*, 18–28.
Lyubetskaya, T., and J. Korenaga (2007a), Chemical composition of Earth's primitive mantle and its variance: 1. Methods and results, *J. Geophys. Res.*, *112*, B03211, doi:10.1029/2005JB004223.
Lyubetskaya, T., and J. Korenaga (2007b), Chemical composition of Earth's primitive mantle and its variance: 2. Implications for global geodynamics, *J. Geophys. Res.*, *112*, B03212, doi:10.1029/2005JB004224.
McDonough, W. F., and S.-S. Sun (1995), The composition of the Earth, *Chem. Geol.*, *120*, 223–253.
McKenzie, D. P., J. M. Roberts, and N. O. Weiss (1974), Convection in the Earth's mantle: Towards a numerical simulation, *J. Fluid Mech.*, *62*, 465–538.
Moore, W. B. (2008), Heat transport in a convecting layer heated from within and below, *J. Geophys. Res.*, *113*, B11408, doi:10.1029/2006JB004778.
Moresi, L., and V. Solomatov (1998), Mantle convection with a brittle lithosphere: Thoughts on the global tectonic styles of the Earth and Venus, *Geophys. J. Int.*, *133*, 669–682.
Moresi, L., and V. S. Solomatov (1995), Numerical investigations of 2D convection with extremely large viscosity variations, *Phys. Fluids*, *7*, 2154–2162.
Nakagawa, T., and P. J. Tackley (2012), Influence of magmatism on mantle cooling, surface heat flow and Urey ratio, *Earth Planet. Sci. Lett.*, *329–330*, 1–10.
Noack, L., and D. Breuer (2014), Plate tectonics on rocky exoplanets: Influence of initial conditions and mantle rheology, *Planet. Space Sci.*, *98*, 41–49.
O'Farrell, K. A., and J. P. Lowman (2010), Emulating the thermal structure of spherical shell convection in plate-layer geometry mantle convection models, *Phys. Earth Planet. Inter.*, *182*, 73–84.
O'Farrell, K. A., J. P. Lowman, and H.-P. Bunge (2013), Comparison of spherical-shell and plane-layer mantle convection thermal structure in viscously stratified models with mixed-mode heating: Implications for the incorporation of temperature-dependent parameters, *Geophys. J. Int.*, *192*, 456–472.
O'Neill, C., and A. Lenardic (2007), Geological consequences of super-sized Earths, *Geophys. Res. Lett.*, *34*, L19204, doi:10.1029/2007GL030598.
O'Neill, C., A. Lenardic, L. Moresi, T. H. Torsvik, and C.-T. Lee (2007), Episodic Precambrian subduction, *Earth Planet. Sci. Lett.*, *262*, 552–562.
O'Neill, C., A. Lenardic, M. Weller, L. Moresi, S. Quenette, and S. Zhang (2016), A window for plate tectonics in terrestrial planet evolution?, *Phys. Earth Planet. Inter.*, *255*, 80–92.
O'Rourke, J. G., J. Korenaga, and D. J. Stevenson (2017), Thermal evolution of Earth with magnesium precipitation in the core, *Earth Planet. Sci. Lett.*, *458*, 263–272.
Padhi, C. M., J. Korenaga, and M. Ozima (2012), Thermal evolution of Earth with xenon degassing: A self-consistent approach, *Earth Planet. Sci. Lett.*, *341–344*, 1–9.
Palme, H., and H. S. C. O'Neill (2003), Cosmochemical estimates of mantle composition, in *Treatise on Geochemistry*, vol. 2, edited by H. D. Holland and K. K. Turekian, pp. 1–38, Elsevier, Amsterdam.
Reese, C. C., V. S. Solomatov, and J. R. Baumgardner (2005), Scaling laws for time-dependent stagnant lid convection in a spherical shell, *Phys. Earth Planet. Inter.*, *149*, 361–370.
Rudnick, R. L., and S. Gao (2003), Composition of the continental crust, in *Treatise on Geochemistry*, vol. 3, edited by H. D. Holland and K. K. Turekian, pp. 1–64, Elsevier.
Rüpke, L. H., J. Phipps Morgan, M. Hort, and J. A. D. Connolly (2004), Serpentine and the subduction zone water cycle, *Earth Planet. Sci. Lett.*, *223*, 17–34.
Salters, V. J. M., and A. Stracke (2004), Composition of the depleted mantle, *Geochem. Geophys. Geosyst.*, *5*, Q05004, doi:10.1029/2003GC000597.
Schubert, G., D. Stevenson, and P. Cassen (1980), Whole planet cooling and the radiogenic heat source contents of the Earth and Moon, *J. Geophys. Res.*, *85*, 2531–2538.
Schubert, G., D. L. Turcotte, and P. Olson (2001), *Mantle Convection in the Earth and Planets*, Cambridge Univ. Press, Cambridge, New York.
Shahnas, M. H., J. P. Lowman, G. T. Jarvis, and H.-P. Bunge (2008), Convection in a spherical shell heated by an isothermal core and internal sources: Implications for the thermal state of planetary mantles, *Phys. Earth Planet. Inter.*, *168*, 6–15.
Silver, P. G., and M. D. Behn (2008), Intermittent plate tectonics?, *Science*, *319*, 85–88.

Smirnov, A. V., J. A. Tarduno, E. V. Kulakov, S. A. McEnroe, and R. K. Bono (2016), Paleointensity, core thermal conductivity and the unknown age of the inner core, *Geophys. J. Int.*, *205*, 1190–1195.
Solomatov, V. S. (1995), Scaling of temperature- and stress-dependent viscosity convection, *Phys. Fluids*, *7*, 266–274.
Solomatov, V. S. (2004), Initiation of subduction by small-scale convection, *J. Geophys. Res.*, *109*, B01412, doi:10.1029/2003JB002628.
Solomatov, V. S., and L.-N. Moresi (2000), Scaling of time-dependent stagnant lid convection: Application to small-scale convection on Earth and other terrestrial planets, *J. Geophys. Res.*, *105*, 21,795–21,817.
Sotin, C., and S. Labrosse (1999), Three-dimensional thermal convection in an iso-viscous, infinite Prandtl number fluid heated from within and from below: Applications to the transfer of heat through planetary mantles, *Phys. Earth Planet. Inter.*, *112*, 171–190.
Stacey, F. D. (1981), Cooling of the Earth—A constraint on paleotectonic hypotheses, in *Evolution of the Earth*, edited by R. J. O'Connell and W. S. Fyfe, pp. 272–276, AGU, Washington, D. C.
Stein, C., J. Schmalzl, and U. Hansen (2004), The effect of rheological parameters on plate behavior in a self-consistent model of mantle convection, *Phys. Earth Planet. Inter.*, *142*, 225–255.
Stein, C., J. P. Lowman, and U. Hansen (2013), The influence of mantle internal heating on lithospheric mobility: Implications for super-Earths, *Earth Planet. Sci. Lett.*, *361*, 448–459.
Stern, R. J. (2005), Evidence from ophiolites, blueschists, and ultrahigh-pressure metamorphic terranes that the modern episode of subduction tectonics began in Neoproterozoic time, *Geology*, *33*, 557–560.
Stevenson, D. J., T. Spohn, and G. Schubert (1983), Magnetism and thermal evolution of the terrestrial planets, *Icarus*, *54*, 466–489.
Tozer, D. C (1972), The present thermal state of the terrestrial planets, *Phys. Earth Planet. Inter.*, *6*, 182–197.
Turcotte, D. L., and G. Schubert (1982), *Geodynamics: Applications of Continuum Physics to Geological Problems*, John Wiley, New York.
Turcotte, D. L., and G. Schubert (2014), *Geodynamics*, 3rd ed., Cambridge Univ. Press, Cambridge, U. K.
Valencia, D., D. D. Sasselov, and R. J. O'Connell (2007), Inevitability of plate tectonics on super-Earths, *Astrophys. J. Lett.*, *670*, 45–48.
van Heck, H. J., and P. J. Tackley (2011), Plate tectonics on super-Earths: Equally or more likely than on Earth, *Earth Planet. Sci. Lett.*, *310*, 252–261.
van Keken, P. E., E. H. Hauri, and C. J. Ballentine (2002), Mantle mixing: The generation, preservation, and destruction of chemical heterogeneity, *Annu. Rev. Earth Planet. Sci.*, *30*, 493–525.
Wasserburg, G. J., G. J. F. MacDonald, F. Hoyle, and W. A. Folwer (1964), Relative contributions of uranium, thorium, and potassium to heat production in the Earth, *Science*, *143*, 465–467.
Weinstein, S. A., and P. Olson (1990), Planforms in thermal convection with internal heat sources at large Rayleigh and Plandtl numbers, *Geophys. Res. Lett.*, *17*, 239–242.
Weller, M. B., A. Lenardic, and C. O'Neill (2015), The effects of internal heating and large scale climate variations on tectonic bi-stability in terrestrial planets, *Earth Planet. Sci. Lett.*, *420*, 85–94.
Wong, T., and V. S. Solomatov (2016), Constraints on plate tectonics initiation from scaling laws for single-cell convection, *Phys. Earth Planet. Inter.*, *257*, 128–136.
Workman, R. K., and S. R. Hart (2005), Major and trace element composition of the depleted MORB mantle (DMM), *Earth Planet. Sci. Lett.*, *231*, 53–72.
Yao, C., F. Deschamps, J. P. Lowman, C. Sanchez-Valle, and P. J. Tackley (2014), Stagnant lid convection in bottom-heated thin 3-D spherical shells: Influence of curvature and implications for dwarf planets and icy moons, *J. Geophys. Res. Planets*, *119*, 1895–1913, doi:10.1002/2014JE004653.
Zindler, A., and S. Hart (1986), Chemical geodynamics, *Annu. Rev. Earth Planet. Sci.*, *14*, 493–571.